MODELRISK

Ecosystem models to support Environmental Risk Assessment of marine ecosystems under HNS spills

Final Report presented to ITOPF

Reporting period: 01/05/2021-30/06/2023

Developed by Irene Martins, Alexandra Guerra, Ana Costa, Fabíola Amorim

CIIMAR- Interdisciplinary Centre of Marine and Environmental Research, University of Porto, Av. General Norton de Matos S/N, 4450-208 Matosinhos, Portugal

Table of Contents

List of Figures

List of Tables

List of Acronyms

4NP	4-nonylphenol
A	Ascendancy
AN	Aniline
B	Biomass
B/P	Biomass to Production ratio
CI	Connectance Index
CFSR	Climate Forecast System Reanalysis
CMEMS	Copernicus Marine Environment Service
CTD	Conductivity, Temperature and Depth (oceanographical instrument)
DW	Dry Weight
EMODNET	European Marine Observation and Data Network product
EE	Ecotrophic Efficiency
EEZ	Exclusive Economic Zone
EPR	East Pacific Rise
ERA	Environmental Risk Analysis
EwE	Ecopath with Ecosim
FCI	Finn's Cycling Index
FG	Functional Groups
GLORYS	Global ocean eddy-resolving reanalysis product
GLS	Generic Length Scale
GPP	Gross Primary Production
HNS	Hazardous and Noxious Substances
IMO	International Maritime Organisation
KS	Keystoneness index
LC_{50}	Median lethal concentration
LS	Lucky Strike hydrothermal vent
MAR	Mid-Atlantic Ridge
MoMar	Monitoring the Mid-Atlantic Ridge Project
MUR	Multi-scale Ultra-high Resolution
MG	Menez Gwen hydrothermal vent
NTB	Nitrobenzene
O	Overhead
OI	Omnivory index
P/B	Production/Biomass ratio
P/R	Production to Respiration ratio
PCE	Tetrachloroethylene (or Perchloroethylene)
PREBAL	Pre-Balanced diagnosis
Q/B	Consumption/Biomass ratio
ROMS	Regional Ocean Modelling System

S	Summer
S10	Seamount 10
SI	Sensitivity Index
SIA	Stable Isotope Analysis
SOI	System Omnivory Index
SST	Sea Surface Temperature
TB	Total Biomass
TE	Transfer Efficiency
TL	Trophic Level
TPP	Total Primary Production
TR	Total Respiration
TST	Total Throughput
W	Winter
WW	Wet Weight

1. INTRODUCTION

Deep-sea ecosystems comprise unique marine environments at the deep ocean (typically below 200 m). Among them, seamounts and hydrothermal vents stand out as captivating and scientifically important ecosystems, characterised by singular features and phenomena.

Seamounts are isolated topographic elevations (i.e., underwater mountains) that rise from the ocean seabed across the world's oceans. These systems, ranging from 100 to >1000 m in height, can be found within tectonic plate areas (intraplate), and are often associated with mid-ocean ridges, back-arc basins and continental slopes [1]. Seamounts are hotspots of biodiversity and one of the major biomes of the global ocean [1-3]. They host a remarkable biodiversity of resident populations of demersal or benthopelagic fishes, which may be of conservation priority or of commercial interest [4]. The complex structure of seamounts results in dynamic water flows that wash off sediments, exposing rocks that are ideal habitat for animals that require hard substrate to grow and attach. Upwelling currents supply nutrients and fuel primary production, consequently supporting the high biodiversity associated with seamounts. Moreover, the complex structure of seamounts also enhances opportunities for foraging, attracting pelagic marine predators that use them as spawning grounds and navigational waypoints, ultimately contributing to the high abundance and species richness of these marine deep-sea ecosystems [5].

Hydrothermal vents are extreme environments, with volcanic vents releasing hot, mineral-rich fluids. They are supported by chemosynthetic processes, where chemoautotrophic microorganisms oxidise inorganic compounds like sulphide, hydrogen, and methane, to produce organic matter [6]. These environments, characterised by extreme conditions, including high temperature and pressure, acidity, and elevated concentrations of toxic chemicals, support rare and endemic species that have adapted to these challenging environments [7]. Endosymbiotic relationships with thiotrophic and methanotrophic bacteria are crucial for the survival and success of biological communities at hydrothermal vent ecosystems [8]. These ecosystems are highly productive, contributing to about 3% of the total organic carbon reaching the deep seabed [9, 10]. In addition to their ecological importance, they have been a source of novel discoveries in biotechnology, including thermophilic microorganisms and bioactive molecules that show potential applications in treating human diseases [11-13]. Furthermore, the unique mineral deposits (e.g., copper, gold, and silver) found at these vents hold significant economic potential [14]. Similar to seamounts, deep-sea hydrothermal vents are typically found along back-arc basins and mid-ocean ridges, including the East Pacific Rise (EPR), the Mid-Atlantic Ridge (MAR), and the Indian Ocean Ridge (IOR) [15].

Hydrothermal vents and seamounts are therefore particularly vulnerable ecosystems to the impacts of anthropogenic activities, potentially posing significant threats to their delicate balance and biodiversity. Moreover, long-term monitoring studies have shown that deep-sea ecosystems are sensitive to climatic variability through its influence on the quantity and quality of surface primary production [2]. These effects may

drive changes on food supply and on the physical environment, resulting in negative impacts on ecosystem services. It is therefore critical to gather a mechanistic understanding on how different stressors effectively affect community structure and function of these fragile ecosystems, to establish baselines for diversity, abundance, biomass, and, ultimately conservation.

In this context, and according to the International Maritime Organisation (IMO), Hazardous and Noxious Substances (HNS) are "any substance other than oil which, if introduced into the marine environment, is likely to create hazards to human health, to harm living resources and marine life, to damage amenities or to interfere with other legitimate uses of the sea" [16].

The increasing number of shipping cargo that transport HNS potentially intensifies a concurrent high risk of accidental spilling at sea [17, 18] (Figure 1). In fact, accidents involving container ships significantly increased in the past decade (2012-2021), with most of them occurring in ports (32.1%) and open seas (29.6%) [18].

Despite valuable efforts to describe HNS [19-22], detect them in marine systems (e.g., through remote sensing [23-26], chemical sensors [27, 28], among others) and assess therein ecotoxicological effects in marine organisms [e.g., 29, 30-33], these chemicals can have different behaviours and patterns after spilled in the ocean, which increases the difficulty of applying effective response countermeasures [18, 34] and robust global regulations regarding HNS liability and compensation [35, 36]. Moreover, these challenges are exacerbated when they affect far-off, hardly accessible and remote deep-sea habitats such as seamounts and hydrothermal vents, as it prevents post-incident long-term monitoring to evaluate environmental, chemical and biological damage of HNS.

HNS can have different behaviours once spilt at the sea, according to the way they are altered during the first few hours after coming into contact with seawater. Predicting HNS behaviour is one of the most important

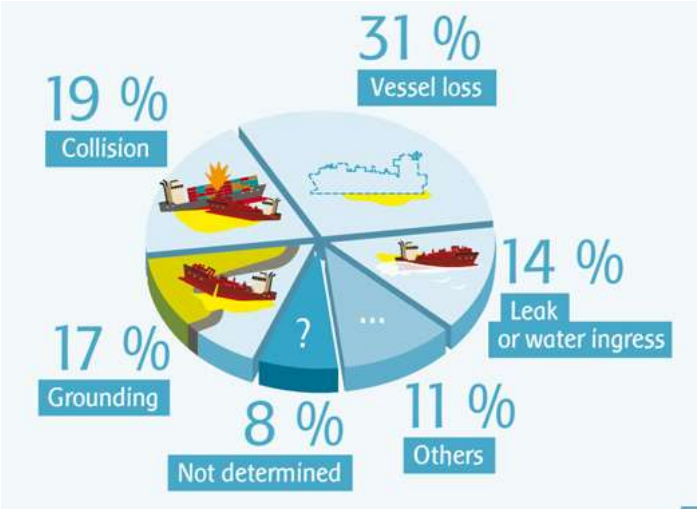

Figure 1. Causes of ship-source accidents involving HNS worldwide from 2005 to 2015 (Source: https://www.chemical-pollution.com/en/sources-pollution/accidental-pollution.php)

stages in the development of a response strategy. According to the Standard European Behaviour Classification (SEBC), the theoretical behaviour of a substance according to its physical and chemical properties lies into one of five main categories: gases (S), evaporators (E), floaters (F), dissolvers (D) and sinkers (S) (Figure 2). Nevertheless, usually a substance does not have one single behaviour but rather several behaviours due to its nature and environmental processes (e.g., wind, waves, current).

To contribute to increase knowledge on this subject, with the MODELRISK project, we aim at developing ecosystem models for Atlantic marine ecosystems, in the Azores region, to predict and quantify the effects of HNS spills on the composition and function of those ecosystems. Specifically, we aim at developing numerical frameworks for Environmental Risk Management (ERA) of HNS spills on marine seamounts and deep-sea hydrothermal vents, and thus, contribute to increased preparedness of responses to accidents with HNS spills at sea. To attain these goals, we propose a numerical framework that incorporates previous work developed by the team on HNS online databases, ocean circulation models, HNS dispersion models, and ecosystem models. This was achieved by incorporating data from the updated HNS CIIMAR online database, the Regional Ocean Modeling System (ROMS), HNS dispersion trajectories and concentrations (OpenOil from OpenDrift), and HNS ecotoxicity effects on food webs of Atlantic seamounts and deep-sea hydrothermal vents, using AQUATOX (US-EPA) and Ecopath with Ecosim, respectively.

The present report describes the methodologies followed, the models' assumptions, limitations and results of the MODELRISK project, achieved between 01/05/2021 and 30/06/2023.

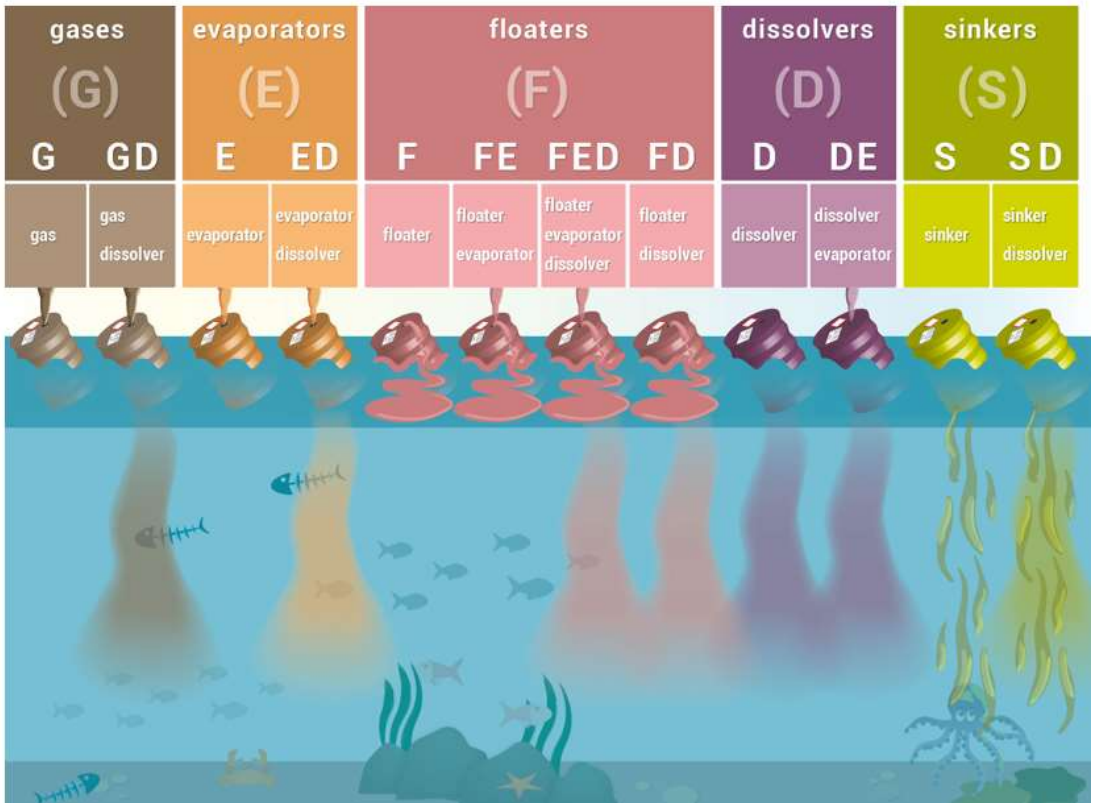

Figure 2. Behaviour of HNS spilt at the sea (Source: http://www.arcopol.eu/_docs/resources/ACT4/FichasENG/Ficha_3_Behaviour_SNPP_EN_web.jpg)

2. MATERIALS & METHODS

Within this section, we present the workflow and provide a brief characterization of the study area (Section 2.1), describe the model configurations utilised for ocean circulation, the Lagrangian modelling tool (Section 2.2), and the food web models (Section 2.3).

The project workflow is summarised in Figure 3. The selection of 4 HNS followed three criteria: i) different behaviour to cover a broader range of representative pathways of HNS dispersion in marine systems (i.e., persistent floater, dissolver, evaporator, sinker), ii) previously existing information regarding HNS fate, weathering, behaviour and toxicity in the CIIMAR database (https://www.ciimar.up.pt/hns/substances.php), and the HNS potential to affect the ecosystems targeted within MODELRISK, i.e., seamounts and deep-sea hydrothermal vent fields. The process of HNS selection is resumed in Table 1, and the selected HNS were 4-Nonylphenol, Tetrachloroethylene, Aniline and Nitrobenzene.

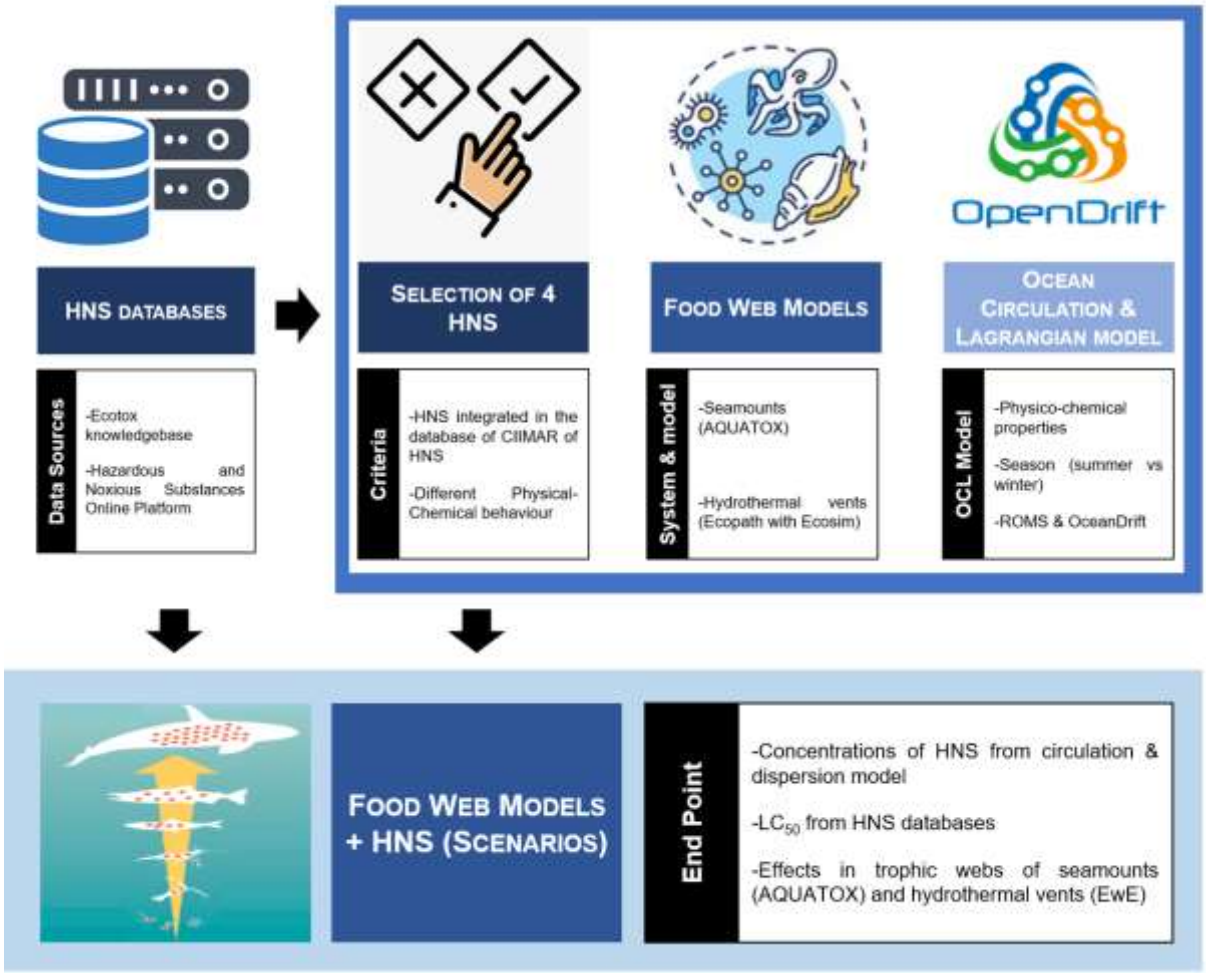

Figure 3. Workflow of MODELRISK project

Table 1. HNS behaviour, presence or absence in the CIIMAR HNS database, and potential effects on seamounts and deep-sea hydrothermal vents. These characteristics guided the initial and final selection of the HNS

Behaviour	HNS initial selection	Present in CIIMAR HNS database	Potential effect on targeted ecosystems	HNS final selection
Persistent floater	**4-Nonylphenol (4NP)**	**Yes**	**Strong effect on pelagic communities**	✓
Dissolver/Evaporator	Acrylonitrile	Yes	Weak effect	⊗
Sinker	**Tetrachloroethylene (PCE)**	**Yes**	**Strong effect on benthos**	✓
Evaporator	Benzene	Yes	Weak or No Effect	⊗
Floater/Evaporator	Styrene	Yes	Weak or No Effect	⊗
Floater/Dissolver	**Aniline (AN)**	**Yes**	**Strong-Medium effect on pelagic and benthic communities**	✓
Floater/Evaporator/Dissolver	Butyl acrylate	Yes	Weak effect	⊗
Sinker/Dissolver	**Nitrobenzene (NTB)**	**Yes**	**Strong-Medium effect on pelagic and benthic communities**	✓

Bold – included in the final selection; ✓ included in the final selection; ⊗ not included in the final selection

We used two different models, AQUATOX (https://www.epa.gov/ceam/aquatox) and Ecopath with Ecosim (EwE, https://ecopath.org/), to represent and simulate food webs in seamounts and hydrothermal vents, respectively. This was necessary as AQUATOX only considers photosynthetic-based primary production. Therefore, for hydrothermal vents, we used EwE to address the primary production derived from the activity of chemoautotrophic bacteria via chemosynthesis.

The ocean circulation (ROMS - Regional Ocean Modelling System; https://www.myroms.org/) & Lagrangian model (OpenDrift; https://opendrift.github.io/) were used to predict dispersion patterns of each HNS within the target area (Azores region), based on their physico-chemical properties and accounting for seasonal differences in circulation (winter vs summer seasons).

Finally, to simulate the toxicological effects of HNS in the trophic webs of seamounts and hydrothermal vents from the Azores region, we used acute toxicity values (LC_{50}), extracted from existing databases (ECOTOX - https://cfpub.epa.gov/ecotox/ - and Hazardous and Noxious Substances Online Platform - https://www.ciimar.up.pt/hns/) and the maximum concentration at the summit of the seamount and at the hydrothermal vent field, outputted from the Ocean Circulation & Lagrangian model.

2.1. Brief description of the study area

The Azores region is located in the North Atlantic Ocean, approximately 1500 Km west of mainland Portugal (Figure 4a and b). The Azores domain is characterised by the Azores Plateau and the Azores archipelago. The Azores archipelago is a group of nine volcanic islands and many small islets that lies on the lateral branch of the Mid-Atlantic Ridge (MAR) near the junction of three major tectonic plates: the North American Plate, the Eurasian Plate and the African Plate (Figure 4a).

This unique location promotes ridge-hotspot interactions with a variation of volcanic processes, fostering iconic and diverse habitats, such as seamounts and hydrothermal field vents. Exceptional combination of geological, hydrodynamic, and geodynamic factors in these deep-sea systems create complex ecosystems, influence nutrient dynamics and offer a diversification of habitats to a wide diversity of marine life forms adapted to thrive in such environments, including deep-sea fishes, corals, sponges, and other invertebrates. Summarily, seamounts and hydrothermal vents contribute to an impressive array of species for the region's remarkable biodiversity.

Based on previous studies for the region [e.g., 5, 37], we verified that four seamounts are present in the area previously calibrated for the circulation models (34.3°/40.8°N, -36°/-28°W), and so good candidates as a representative seamount ecosystem from the NE Atlantic located within the area calibrated by the circulation model (Table 2). Due to a lower depth location of the summit (413 m), we have selected seamount 10 as the site to implement the seamount model.

Regarding the hydrothermal vent fields, three of the largest hydrothermal vent fields were good candidates within the area previously calibrated for the circulation models (Table 2). Due to a lower depth location (850 m), we have selected Menez Gwen as the reference site to implement the hydrothermal vent model. The hydrothermal activity at MG is concentrated in small areas, particularly on a small volcano at the central top region of the field [38]. The temperature of the diffuse fluids ranges from 10 to 56°C, while the hottest fluid escapes from chimneys at approximately 284°C [39]. The *in situ* pH is acidic (4.2-4.9), and the hydrothermal fluids contain high concentrations of gases such as CO_2, CH_4, and H_2S [40, 41].

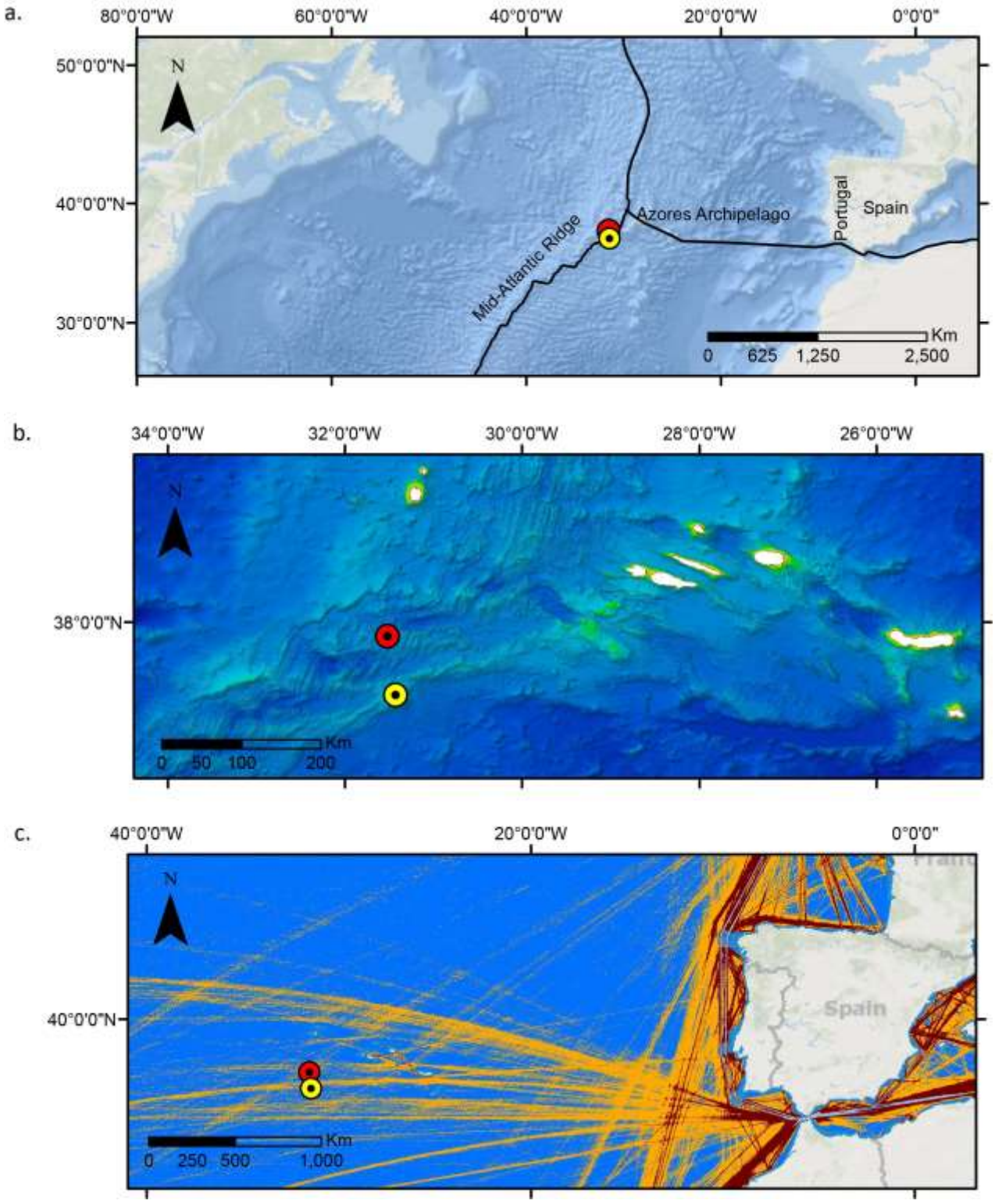

Figure 4. Study area. a) General overview of the study area (black lines - tectonic limits) (Service Layer Credits: GEBCO, NOAA, Esri, National Geographic, Garmin, HERE, Geonames.org, and other contributors); b) Detail of the study area (Service Layer Credits: EMODNET); c) Density of shipping maritime routes (Service Layer Credits: EMODNET). Yellow dot – Seamount 10; Red dot – Menez Gwen hydrothermal vent

Table 2. Characteristics of the candidate four seamounts and three hydrothermal vents present in the area previously calibrated for the circulation model

Seamount number	Longitude (°W)	Latitude (°N)	Depth of summit (m)	Height (m)	Final selection
10	**-31.4322**	**37.1774**	**413**	**1305**	✓
21	-31.4990	37.8287	824	1129	⊗
22	-31.2151	37.8621	707	1454	⊗
31	-31.0231	38.3213	712	1197	⊗
Hydrothermal vent	**Longitude (°W)**	**Latitude (°N)**	**Depth (m)**		**Final selection**
Lucky Strike	-32.2833	37.3000	1100		⊗
Menez Gwen	**-31.5247**	**37.8416**	**850**		✓
Rainbow	-33.9019	36.2297	2300		⊗

Bold – included in the final selection; ✓ included in the final selection; ⊗ not included in the final selection

In addition, the Azores region is crossed by several important marine shipping routes. These routes serve as vital connections across the Atlantic, including vital connections between the east coast of North America and western Europe, fuelling the transatlantic trade through the transportation of goods, commodities, and containers between these continents. Given its strategic position, the Azores region also serves as a waypoint for ships undertaking longer voyages, as a convenient stopover point or to benefit from favourable currents and winds in the area (Figure 4c).

2.2. Ocean circulation & Lagrangian modelling tool

2.2.1 Regional Ocean model configuration

The ocean numerical model adopted for the present study is the Regional Ocean Modelling System (ROMS), previously implemented for the Azores region in a two-way online nesting capability, considering a parent grid with 3 km horizontal resolution and a child grid with 1 km horizontal resolution (Figure 5), covering the regions of the selected hydrothermal vent and seamount. Both grids considered 30 vertical levels defined with stretched S-coordinates.

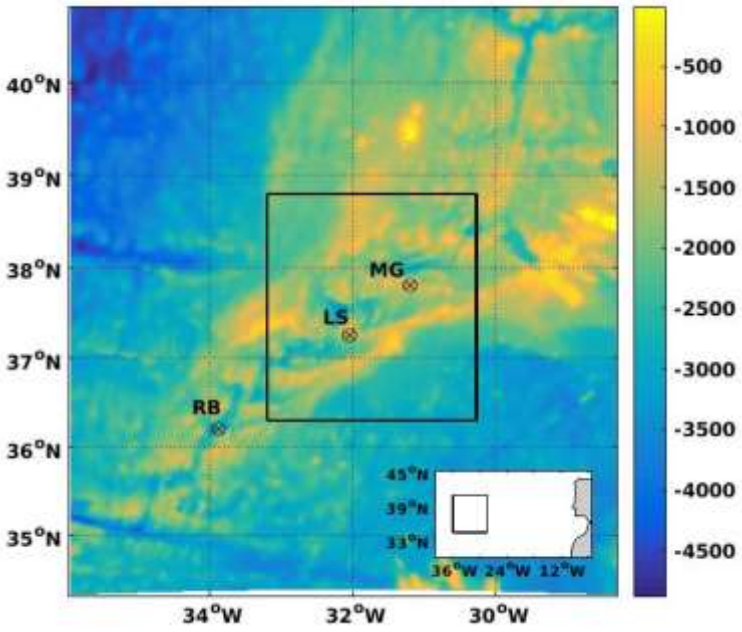

Figure 5. Parent grid domain (3 km resolution). The location of the hydrothermal field of Menez Gwen (MG), Lucky Strike (LS) and Rainbow (RB) are presented. The rectangular area represents the child grid domain (1 km resolution)

The parent grid was off-line nested into the global ocean eddy-resolving reanalysis product (GLORYS) from the Copernicus Marine Environment Service (CMEMS), which provided the initial and daily boundary conditions (temperature, salinity, elevation and velocities). The child grid was nested online in the parent grid, which provides the temperature, salinity, elevation and velocities each time step at the contact layer.

The vertical mixing, momentum and tracers were parameterized with the Generic Length Scale (GLS), fourth-order horizontal advection and third-order upwind advection schemes. The barotropic tidal forcings were considered, derived from the TPXO datasets [42].

Wind and surface fluxes were derived from the Climate Forecast System Reanalysis (CFSR, [43]), and internally calculated for both grids using the bulk formulation. The bathymetry for both grids was derived from the European Marine Observation and Data Network product (EMODNET), with approximately 200 m resolution, which provides a good representation of the sea bottom contours. Model results were validated against a series of observational data.

Note that the two study regions selected as test cases to represent the impact of HNS spills, the Menez Gwen hydrothermal vent and Seamount 10, are located within the child domain, which is completely covered by the configuration with the ROMS circulation model.

2.2.2 Semi-Lagrangian

In the first phase of the project, when we were defining which lagrangian tool could best describe the HNS behaviour from a deep-sea spillage, we chose the OpenOil tool which is part of the OpenDrift Package (https://opendrift.github.io/). However, throughout the simulations, we realised that the 2 heavier HNS selected, tetrachloroethylene and the nitrobenzene, did not sink during the simulation, but instead flowed to the surface and dispersed. After contacting the package developers (namely Dr. Knut-Frode), they explained that the OpenOil, which is based on the PyGnome oil spill model from the Office of Response and Restoration from NOAA (National Oceanic and Atmospheric Administration) was not numerically prepared to deal with substances heavier than the ocean water (> 1025 kg m^{-3}), and suggested to use the sub-model OceanDrift instead, since this sub-model is the core of OpenDrift package and suitable for passive tracers or objects that flow with the ocean current, which may be subject to an additional wind drag.

With OceanDrift, it is possible to build our own module subclassing, implementing the relevant processes based on provided forcing data from the ocean model (temperature, salinity, density, etc.). Indeed, based on the OceanDrift sub-model, we were able to update the terminal velocity of the droplets (Lagrangian elements) that represent a parcel of the total volume of each HNS, by adding the same formulation used in the OpenOil sub-model, based on [44]. With this formulation, the terminal velocity of each droplet is updated through the ocean numerical grid domain (Eulerian field), each time step, based on the local density, calculated from model temperature, salinity and depth (D = f(T,S,Z)).

The processes involving the fate of a substance in the water environment occurs in two different phases, the Near-field and the Far-field. In the Near-field phase, the first part of the plume is under the influence of the momentum and mixing inside the plume, due to the water entrainment. The space-time extension of this domain is of the order of hours and a few hundred meters. In the Far-field, the plume reaches a neutral buoyancy level, the momentum is negligible and the passive advection and diffusion becomes the dominant processes to the plume behaviour and fate. Regarding a deep-sea release, each HNS will behave as parcels of a number of droplets, following the ambient current and parameters (e.g., water temperature and salinity), reaching the ocean floor or surface due to their buoyancy. In this work, we considered only the second phase of the release, the Far-field, due the spatio-temporal resolution of the ocean model, which is not enough to describe processes of order of few meters and hours, and since we are interested on the fate of the HNS droplets through the water column due to the local hydrodynamics.

Regarding the weathering processes, they are not accounted for in OceanDrift. The simulated accidents describe the leakage, during the first 5 days of HNS from the containers at the seabed (after sinking), where weathering processes are usually not considered (e.g. Gnome, HNS-MS). The Lagrangian sub-model computes the displacement of each HNS particle under the combined effect of the wind, currents and sub to mesoscale features, related to the circulation and local topographic constraints, which is well represented by the oceanic model, considering the adopted resolution and parameterization. In addition, the Lagrangian sub-model

computes the buoyancy effect, the turbulent diffusive transport, the vertical dispersion into the water column and the horizontal spreading, with all processes being also satisfactorily resolved by the ocean model resolution and parameterization. This approach was the same as the one adopted by the HNS-MS European Project (https://www.hns-ms.eu/) and GNOME spill model (https://github.com/NOAA-ORR-ERD/PyGnome).

To simulate the different HNS spills (Table 3), we followed [45] and considered a controlled leakage from an accident at sea involving 100 containers with a volume of 76 m^3 each, which sank to the seabed. A total volume of 7600 m^3 (100 containers x 76 m^3) leaked during five days (120 h) from the containers, which were considered to be uniformly distributed around the Menez Gwen hydrothermal vent (MG) and the Seamount 10 (S10), for each seasonal scenario (winter vs summer). We considered the total volume of each HNS equally distributed in 12.000 droplets, with a diameter of 0.3 mm. Each droplet is fully passive and represents a parcel of the released HNS including the substances dissolved in it. The use of passive tracers to study pollutant dispersion is common practice in coastal modelling studies (HNS-MS) [46-48]. Each simulation ran for 10 days with an hourly output.

Table 3. Density of the selected HNS

HNS	Density (Kg m^{-3})
4NP	950
Aniline	1020
Tetrachloroethylene	1620
Nitrobenzene	1203

2.3. Ecosystem and Food web models

2.3.1. Seamounts

2.3.1.1. Ecological structure

The final seamount food web model comprises 15 different groups (Figure 6). The functional groups aggregation process followed the work conducted by [49], as well as the feedback provided by our external consultors from OKEANOS (University of Azores, Portugal), experts on deep-sea ecology. Hence, the final number of functional groups accounted for in the seamount food web resulted from a comprehensive process that included calculations, estimations, and professional judgement, to ensure a trade-off between a fair representation of the existing trophic interactions and the need for balancing complexity and pragmatism throughout the modelling process. Moreover, the criteria for the aggregation of functional groups have also considered the representativeness of endemic and commercially important species (e.g., tuna) of the Azores seamounts (Figure 7).

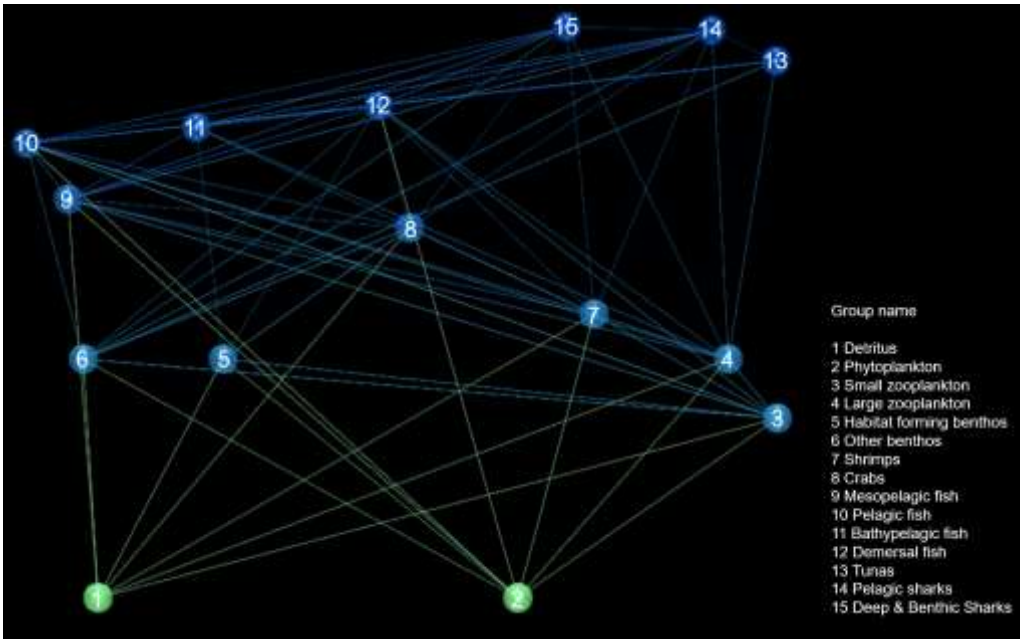

Figure 6. Considered seamount food web constructed based on the work from Morato et al., 2016 and on the advisory of project consultants' expert judgement

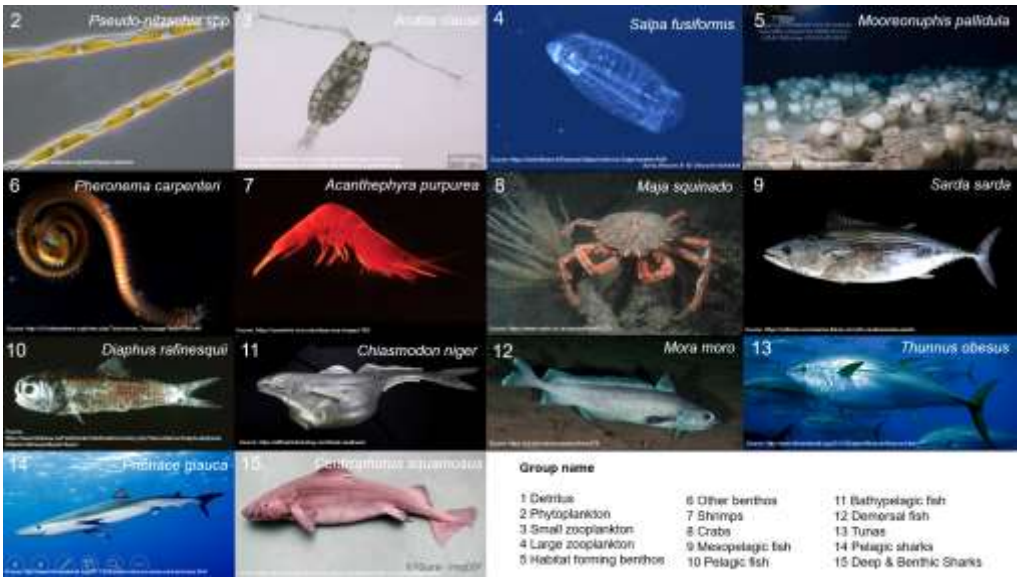

Figure 7. Illustration of the representative species of each functional group considered in the seamount food web model

The initial values of biomass for each biotic group considered the ones reported by [49]. In newly formed groups resulting from aggregation of groups reported in [49], biomass values are an algebraic sum of the single group biomass (Table 4). The calculation of the trophic relations established between the functional groups, i.e., construction of the trophic matrix for the seamount food web model, followed the estimations of [49]. In the case of newly created groups, these estimations were properly normalised to meet the model criteria (sum of prey = 1).

Table 4. Biotic groups, representative species of each group (endemic and commercially important) and biomass considered in the seamount food web model

Group	Group name	Representative species	Biomass ($g\ m^{-2}$)
Phytoplankton	Phytoplankton	*Pseudo-nitzchia spp.*	0.580
Zooplankton	Small zooplankton	*Acatia clausii*	0.904
Zooplankton	Large zooplankton	*Salpa fusiformis*	0.767
Benthic invertebrate	Other benthos	*Mooreonuphis pallidula*	0.448
Benthic invertebrate	Habitat forming benthos	*Pheronema carpenteri*	0.442
Benthic invertebrate	Shrimp	*Acanthephyra purpurea*	0.459
Benthic invertebrate	Crabs	*Maja squinado*	0.406
Fish	Pelagic fish	*Sarda sarda*	0.128
Fish	Mesopelagic fish	*Diaphus rafinesquii*	0.196
Fish	Bathypelagic fish	*Chiasmodon niger*	0.135
Fish	Demersal fish	*Mora moro*	0.238
Fish	DeepWaterAndBenthic Sharks and Rays	*Centrophorus squamosus*	0.002
Fish	Pelagic sharks	*Prionace glauca*	0.010
Fish	Tunas	*Thunnus obesus*	0.018

2.3.1.2. The AQUATOX model: implementation and parametrization

The ecosystem-level model AQUATOX, developed by US-EPA, is a mechanistic model, suitable to assess the effects of several stressors (e.g., environmental variables, contaminants) at the ecosystem level because it accounts for the trophic relationships among the different species or groups present in the food web, from primary producers to fish [50-52]. Besides the food web model, an ecotoxicology sub model is also embedded in AQUATOX, which simulates the lethal and sub-lethal toxic effects of chemicals in the organisms that comprise the food web, as long as the specific ecotoxicological parameters are supplied to the model. Subsequently, a sequence of computations estimates the biomass of organisms being lost through lethal toxicity and the factors that relate sublethal toxicities to the lethal toxicity [for more details on mathematical formulation see 51, 52, 53]. Due to these particularities, AQUATOX was chosen to implement the seamount model within the MODELRISK project.

The AQUATOX model requires the input of a battery of parameters to describe each group. Despite the changes in the final considered trophic groups resulting from the aggregation process previously described, most groups conserve the same reference species as the original paper from [49], which allowed us to take advantage of previous calibration efforts. Moreover, further research took place and allowed compiling valid data to complement physiological (e.g., fish length and/or weight), ecological (e.g., tolerance to low levels of dissolved oxygen; tolerance to high levels of ammonia), and life cycle (e.g., longevity) parameters into the dataset and, therefore, parameterise the model.

Missing data was retrieved from databases freely available online, such as Fishbase (https://www.fishbase.se/search.php; https://www.sealifebase.ca/home.htm) and life cycle expectancy (https://www.worldlifeexpectancy.com/fish-life-expectancy; https://genomics.senescence.info/species/index.html). Some of the gaps in data used data from other models available in the literature as a proxy. With this, we were able to calculate fish swimming speed (https://www.fishbase.se/manual/english/PDF/FB _Book_ATorres_Swimming_Speed_RF_JG.pdf) and weight through allometric equations ($W = aL^b$), such as the length(L)-weight(W) relationship and function parameters (a; b). For invertebrates, we used population models [54].

Whenever specific parameters were missing or unavailable, we considered default values from AQUATOX. This methodology is valid as we have selected the most similar species available in AQUATOX libraries upon model set-up in relation to the species accounted for in the seamount food web.

After fine-tuning the model, we compared the abiotic model results with data from Copernicus Marine Service (https://marine.copernicus.eu/), to evaluate model output against environmental physico-chemical characteristics. Monthly data of water temperature and salinity were obtained for the period between 16/01/2019 and 16/01/2020 from a reanalysis product (GLOBAL_MULTIYEAR_PHY_001_030; Dataset: cmems_mod_glo_phy_my_0.083_P1M-m).

Conversely, monthly biogeochemical data, such as nitrate, phosphate, and dissolved oxygen, were also obtained for the same time period, but from a hindcast product (GLOBAL_MULTIYEAR_ BGC_001_029; Dataset: cmems_mod_glo_bgc_my_0.25_ P1M-m).

2.3.1.3. Sensitivity analysis

To assess the sensitivity of the model's outputs to changes in the input parameters, we performed a local sensitivity analysis. By systematically varying the values of individual parameters while keeping others constant, sensitivity analysis provides insights into the relative importance and influence of different parameters on the model's outcomes. In the context of this study, the local sensitivity analysis involved varying the values of the parameters by ±10% from their baseline values, allowing for an evaluation of the resulting impacts on the model outputs. This analysis aids in highlighting the most sensitive parameters, which are the ones that require a most accurate estimation from empirical works, followed by a careful model calibration. Parameter's sensitivity was estimated by the formula:

$$SI = \frac{100}{p \cdot n} \cdot \sum_{i=1}^{n} \frac{\left| X_i - X_i^{ref} \right|}{X_i^{ref}}$$

Where, p is variation of the parameter (±10%), n is total duration of the simulation (days), X_i is the new value of the state variable and X_i^{ref} is the reference value of the state variable.

2.3.1.4. Simulating HNS spill scenario – S10

To simulate the HNS spill scenario in Seamount 10, we considered the acute toxicity values (LC_{50}) for each functional group, which are available in existent databases (ECOTOX and CIIMAR's HNS database), as well as the maximum concentration at the summit of seamount (413 m; Table 2), during the 10-day simulation of the ocean circulation (ROMS) and Lagrangian model (OpenDrift) (Figure 8).

The ecotoxicological data for some of the four considered Hazardous and Noxious Substances (HNS) and/or the seamount-specific functional groups were not always readily available. In such instances, we utilized the available data for the closest taxonomic group associated with the same HNS. When data for a particular HNS and functional group pairing was not found, we opted for selecting available data for a similar HNS that exhibited a similar behaviour upon contact with seawater. The data used as inputs for AQUATOX are in Table 5.

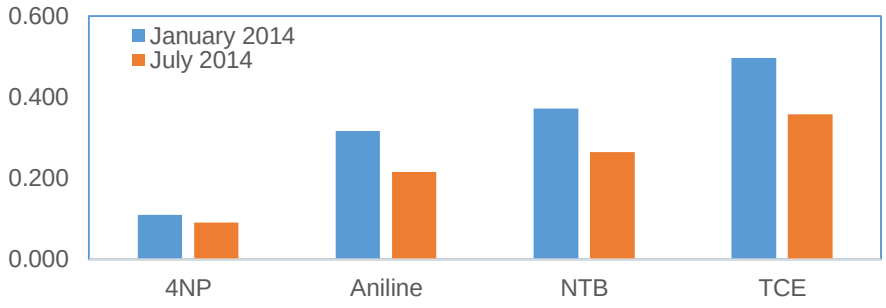

Figure 8. Maximum concentration of the four HNS at the summit of seamount (mg/L) - outputted data from the ocean circulation & Lagrangian model

Table 5. Ecotoxicological data used for the functional groups of the seamount food web model

				4NP			Aniline			Nitrobenzene			Tetrachloroethylene		
#	Group	Group name	Reference species	LC50(mg/L)	LC50(µg/L)	LC50 - exposure time (h)	LC50(mg/L)	LC50(µg/L)	LC50 - exposure time (h)	LC50(mg/L)	LC50(µg/L)	LC50 - exposure time (h)	LC50(mg/L)	LC50(µg/L)	LC50 - exposure time (h)
1	Phytoplankton	Phytoplankton	*Pseudo-nitzschia* spp.	NA	27-2500[1]	96h	183.9	183900	288-312 (12-13 days)	0.76	760	96	0.76	760	96
2	Zooplankton	Small zooplankton	*Acartia clausi*	2.8	2800	48	11	11000	48	7.6	7600	96	13.2	13200	96
3	Zooplankton	Large zooplankton	*Salpa runcinata*	0.015	15	24	0.015	15	24	0.015	15	24	0.015	15	24
4	Benthic invertebrate	Habitat forming benthos	*Mooreonuphis pallidula*	3.03	3030	24h	12	12000	96	0.057	57	96	0.057	57	96
5	Benthic invertebrate	Other benthos	*Pheronema carpenteri*	2.5	2500	48	15	15000	96	29	29000	96	1.3	1300	96
6	Benthic invertebrate	Shrimp	*Acanthephyra purpurea*	89.5	89500	48	2.3	2300	96	2.14	2140	96	17.4	17400	96
7	Benthic invertebrate	Crabs	*Maja squinado*	100	100000	48	0.8	800	96	2.9	2900	96	2.9	2900	96
8	Fish	Pelagic fish	*Sarda sarda*	6	6000	96	78.4	78400	96	1.2	1200	48	9.6	9600	96
9	Fish	Mesopelagic fish	*Diaphus rafinesquii*	1.8	1800	96	1.8	1800	96	1.4	1400	96	1.4	1400	96
10	Fish	Bathypelagic fish	*Chiasmodon niger*	6	6000	96	78.4	78400	96	1.2	1200	48	9.6	9600	96
11	Fish	Demersal fish	*Mora moro*	6	6000	96	78.4	78400	96	1.2	1200	48	9.6	9600	96
12	Fish	Benthic&Deep water sharks	*Centrophorus squamosus*	0.9	900	96	43.2	43200	60	0.55	550	96	5.84	5840	96
13	Fish	Pelagic sharks	*Prionace glauca*	0.9	900	96	43.2	43200	60	0.55	550	96	5.84	5840	96
14	Fish	Tunas	*Thunnus obesus*	0.9	900	96	43.2	43200	60	0.55	550	96	5.84	5840	96

2.3.2. Hydrothermal vents

2.3.2.1. Ecological structure

The composition of the biological community at the Menez Gwen (MG) vent field is described in a considerable number of previous works. The dominant species in the hydrothermally active sites of Menez Gwen (MG) is the vent mussel *Bathymodiolus azoricus*, along with two gastropod species, *Lepetodrilus atlanticus* and *Protolira valvatoides* [38, 41, 55, 56]. Important populations of the shrimp species *Mirocaris fortunata* and *Rimicaris chacei* can also be found on active deposits and among the *B. azoricus* mussels [41, 55]. The dominant indigenous predator in this ecosystem is the vent crab *Segonzacia mesatlantica* [57].

Meiofauna, which refers to organisms smaller than 250 µm, constitute a significant portion (57-76%) of the relative faunal abundance in MG, with copepods being the primary constituents of the meiofauna [41, 58]. Based on information retrieved from the above mentioned works, 8 functional groups were considered to described the MG food web:

- 5 consumer groups: "vent Mussels" (*Bathymodiolus azoricus*), "Copepods" (representing the meiofauna with Copepoda and Nauplii), "vent Gastropods" (including *Lepetodrilus atlanticus* and *Protolira valvatoides*), "vent Shrimps" (*Mirocaris fortunata* and *Rimicaris chacei*), and "vent Crabs" (*Segonzacia mesatlantica*);
- primary producer group: "Free-living bacteria,"
- detritus groups: "Marine Snow" and "Benthic detritus".

2.3.2.2. The EwE model: implementation and parametrization

The Ecopath with Ecosim (EwE) software was used to model the food web of the Menez Gwen vent field. This software employs a mass-balance approach to estimate energy and nutrient flows among different trophic levels [59]. The model's parameterization is based on the assumption of mass balance over a specified time period, typically one year, and relies on two master equations:

$$\boldsymbol{B_i \times \frac{P_i}{B_i} = \sum_{j=1}^{n} B_j \times \frac{Q_j}{B_j} \times DC_{ij} + B_i \times \frac{P_i}{B_i} \times (1 - EE_i) + Y_i + E_i + BA_i} \quad (1)$$

$$\boldsymbol{B_j \times \frac{Q_j}{B_j} = B_j \times \frac{P_j}{B_j} + B_j \times \frac{R_j}{B_j} + \frac{U_j}{Q_j} \times B_j \times \frac{Q_j}{B_j}} \quad (2)$$

The first equation (Eq. 1) establishes the connection between the organic matter budget of prey groups (**i**) and their corresponding predator groups (**j**) in the food web. It considers various factors such as production (**P**),

biomass (**B**), consumption (**Q**), diet composition (**DC**), ecotrophic efficiency (**EE**), mortality (**1-EE**), fishery catch (**Y**) (EwE was initially developed for fished species), export (**E**), and biomass accumulation (**BA**) [60].

The second master equation (Eq. 2) ensures energy balance within groups and links the consumption of predator groups to their production, incorporating terms for respiration (**R**) and unused consumption (**U**) [60].

Before balancing the model, a Pre-Balanced (PREBAL) diagnosis was conducted to identify any inconsistencies in the model structure and data quality. Vital rates of organisms, including consumption, production, and respiration, were analysed to ensure they followed basic physiological restrictions [61].

The diet composition of each group in the food web (Table 6) was primarily determined using relevant literature sources. However, due to data gaps, the diet composition was considered the least reliable parameter and was adjusted during the balancing process [60].

Table 6. Balanced diet compositions (DC) for each compartment of the MG food web model

	Prey \ predator	1	2	3	4	5
1	vent Crabs					
2	vent Shrimps	0.09				
3	vent Gastropods	0.35	0.2			
4	Copepods		0.1	0.1	0.05	
5	vent Mussels					
7	Free-living bactéria		0.3	0.5	0.7	0.49
8	Marine Snow			0.05	0.25	0.01
9	Benthic detritos	0.56	0.4	0.35		
	Import					0.5

Diets of each functional group were normalised to 1

During the balancing process, adjustments were made to the diet compositions to achieve EE values lower than 1, as required by the software. Output values of the balanced model, such as biomass and productivity, were compared to data from other deep-sea vent ecosystems to assess the model's accuracy [62, 63], due to the lack of information for the study site.

The Ecosim component of the model represents the ecosystem dynamics over time. It utilises initial conditions and parameter definitions from Ecopath and is based on differential equations such as Eq. 3 [59, 64, 65]:

$$dB_i / dt = gi \times \Sigma j\, Qji - \Sigma j\, Qij + Ii - (MOi + Fi + ei) \times Bi \quad (3)$$

where, **I** is the extent of immigration; **MO** is the non-predation rate of natural mortality; **F** is the fishing mortality and **e** the emigration.

The concept of the foraging arena is incorporated to model prey-predator interactions (Eq. 4), allowing fine-tuning of model responses.

$$Qij = \frac{aij \times vij \times Bi \times Bj}{2 \times vij \times aij \times Bj} \quad (4)$$

Where **v** is the vulnerability and **a** is the effective search rate.

Vulnerability and effective search rates are key parameters that shape predator-prey functional responses [66]. In this study, vulnerability parameters were set differently for top predator groups ("vent Crabs") and other groups (1.1 for the “vent Crabs” group and 2.0 for all the other groups). The feeding time adjust rate depended on the behavioural characteristics of the functional groups. Thus for “vent crabs” the feeding time adjust rate was set at 0.1, because predation mortality risk was assumed to be very low for this group, and consequently, the feeding time was considered constant. For the “vent Mussels” group, as sessile organisms, a feeding factor of 0 was assigned. For all the other groups, the “feeding time adjust rate” was set at 1, assuming that these groups exhibit behavioural mechanisms to decrease predation risks, such as taking advantage of the shelter provided by mussels [9].

2.3.2.3. Simulating HNS spill scenarios at Menez Gwen

To simulate HNS spill scenarios at the Menez Gwen hydrothermal vent field, we considered the acute toxicity values (LC_{50}) for each functional group, which is available in existent databases, as well as the maximum concentration at the depth of the hydrothermal vent (850 m; Table 2), during the 10-day simulation of the ocean circulation (ROMS) and Lagrangian model (OpenDrift) (Table 7).

According to the dispersion model results, the concentration of tetrachloroethylene (PCE) at the MG hydrothermal vent field, exceeds the LC_{50} values for certain functional groups, specifically the "vent Gastropod" and "vent Mussels," during both summer and winter seasons (Table 7).

We have, thus, used the Ecosim model to simulate the effects of the worst-case scenario (i.e., the scenario with the highest PCE concentration that corresponded to the summer PCE spill, as shown in Table 7, to assess the effects of PCE on MG food web.

To include the effect of LC_{50} in the two groups from the MG food web with a LC50 specific value lower than the simulated PCE concentration, we had to use a proxy approach, since the model has no explicit way to account for this. Thus, to overcome this limitation, we used the "other mortality" parameter (M0 in Eq. 3) as a Forcing Function (FF), in the Ecosim module. Specifically, we estimated a coefficient that modified M0 (a M0 multiplier, registered in Table 8) in order to cause a 50% reduction in the biomass of the affected group. The F) was introduced to the Ecosim module during the first month of the second year of simulations to enhance data interpretation. The M0 multiplier remained set to 1 for the remaining months, before and after the accident simulation, in order to nullify the effect of the FF. The simulations ran over a 20-year period.

Table 7. HNS maximum concentrations (mg L^{-1}) for winter (W) and summer (S) at the Menez Gwen area and assumed acute toxicity values (LC_{50}) for each functional group. 4NP: 4-Nonylphenol; AN: Aniline; NTB: Nitrobenzene; PCE: tetrachloroethylene; Shaded in black correspond to LC_{50} values below predicted HNS concentrations at the MG vent field

[HNS] $_{maximum}$ simulated		**4NP**	**AN**	**NTB**	**PCE**
		W - 0.24 S - 0.22	W - 0.59 S - 0.60	W - 0.88 S - 1.06	W - 1.18 S - 1.43
[LC_{50}] $_{reference}$ Functional Group	vent Crabs	2.01	29.4	2.9	17.4
	vent Shrimps	0.30	29.4	44	17.4
	vent Gastropods	18.00	18	170	**1.1**
	Copepods	0.75	11	7.6	13.2
	vent Mussels	3.00	9.5	110	**1.1**

Table 8. Input parameters for scenario simulation in Ecosim: FG – functional groups; M0 multipliers - coefficients applied to 'other mortality'; PCE - Tetrachloroethylene

FG	M0 multipliers
	PCE
1 - vent Crab	-
2 - vent Shrimp	-
3 - vent Gastropod	11.90
4 – Copepods	-
5 - vent Mussels	35.30

**"Free-living bacteria" are not being included in this methodology due to a total lack of data regarding the effects of HNS on this group.*

However, the "Free-living bacteria" group was not subjected to this procedure due to a lack of data regarding the effects of HNS on this group. On the other hand, bacteria tend to have a high resistance to toxic substances [67, 68]. Therefore, it was considered reasonable not to include the "Free-living bacteria" group in this procedure.

3. RESULTS

3.1. Ocean & Lagrangian model

3.1.1. Regional Ocean model

The results of the regional ocean model showed that with the vertical mixing scheme adopted together with the topography parameterization (e.g., high-resolution data and smoothing), horizontal resolution and vertical layer discretization, the model is able to reproduce deep-sea submesoscale processes (order 1-10 km) related to complex bathymetric systems, as submarine ridges, seamounts and canyons [69-73]. Moreover, the results were successfully validated with CTD records from 2014 for Lucky Strike (LS) hydrothermal vent field (also within the child domain) (Figure 9), collected in the region as part of the Monitoring the Mid-Atlantic Ridge project (MoMar; www.interridge.org/node/163), as well as with absolute dynamic topography and geostrophic velocity from AVISO (www.marine.copernicus.eu), thermohaline variability structure from ARGO floats, SST from the Multi-scale Ultra-high Resolution (MUR) SST (https://podaac.jpl.nasa.gov/dataset/MUR-JPL-L4-GLOB-v4.1) and vertical temperature data from CORA (http://www.coriolis.eu.org/Data-Products/Products/CORA).

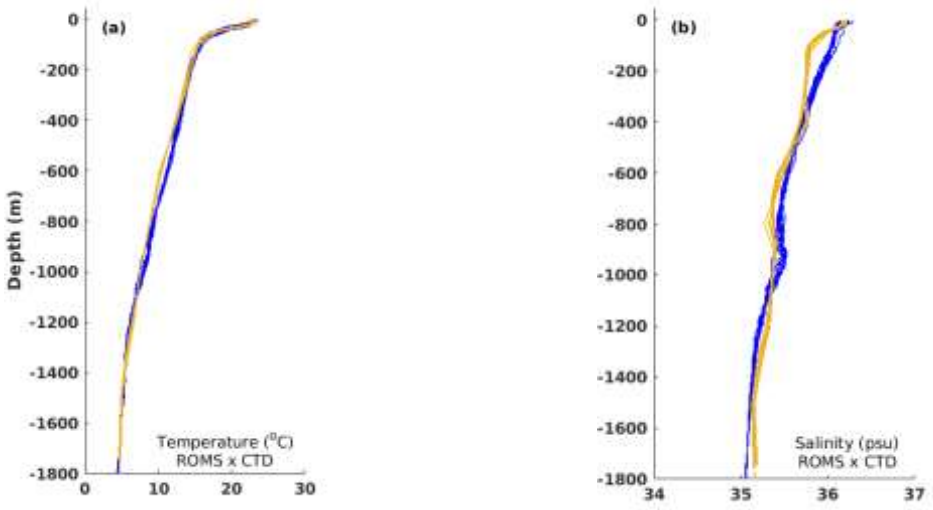

Figure 9. Observed (blue) and modelled (yellow) depth profilers of temperature (a) and salinity (b) over the LS hydrothermal vent.

3.1.2. HNS dispersion

The results of the Lagrangian model for each considered HNS are presented in terms of the hourly concentration in the MG area and at the S10 summit, and the final position and concentration on the seafloor for the sinkers HNS (tetrachloroethylene and nitrobenzene), as the floaters (aniline and 4-nonylphenol) rapidly ascended to the sea surface and the concentrations at MG and the S10 summit decreased to 0 (Figure 10 and Figure 13).

3.1.2.1. HNS dispersion – Menez Gwen (MG)

The hourly concentration of the tetrachloroethylene (PCE) and nitrobenzene (NTB) at MG (Figure 10) was higher during the first three days, for the July scenario (PCE max. concentration July = 1.432 mg L^{-1}; NTB max. concentration July = 1.064 mg L^{-1}). In January, the concentrations of PCE and NTB remained higher during leakage, from January 12 until January 15, and started decreasing only on January 16. However, the simulated concentrations of PCE and NTB in January were lower than in July (PCE max. concentration January = 1.180 mg L^{-1}; NTB max. concentration January = 0.884 mg L^{-1}).

Aniline was more persistent in the water column than 4NP, which reflects its higher density compared to 4NP, but both HNS reached the surface during the leakage period of 5 days.

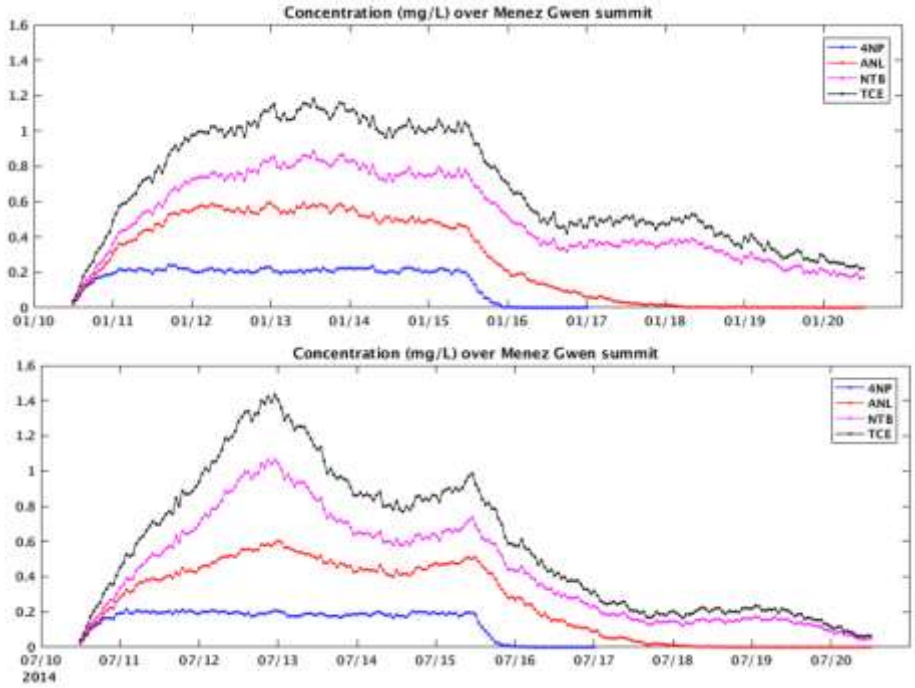

Figure 10. Hourly concentration of the selected HNS, over the MG summit, during the months of January (upper panel) and July (lower panel)

The final position of the NTB (Figure 11) shows the tendency of the HNS droplets to settle down at the deeper locations that surround the MG vent field. During January the dispersion was elongated and reached a wider area, while during July the dispersion showed a circular behaviour around the seafloor that surrounds the MG. These results highlight the capacity of the model to represent the different features of the local circulation. Following the behaviour presented in Figure 10 and the local circulation, the higher final concentration of the Nitrobenzene was observed during January and close to the MG hydrothermal vent.

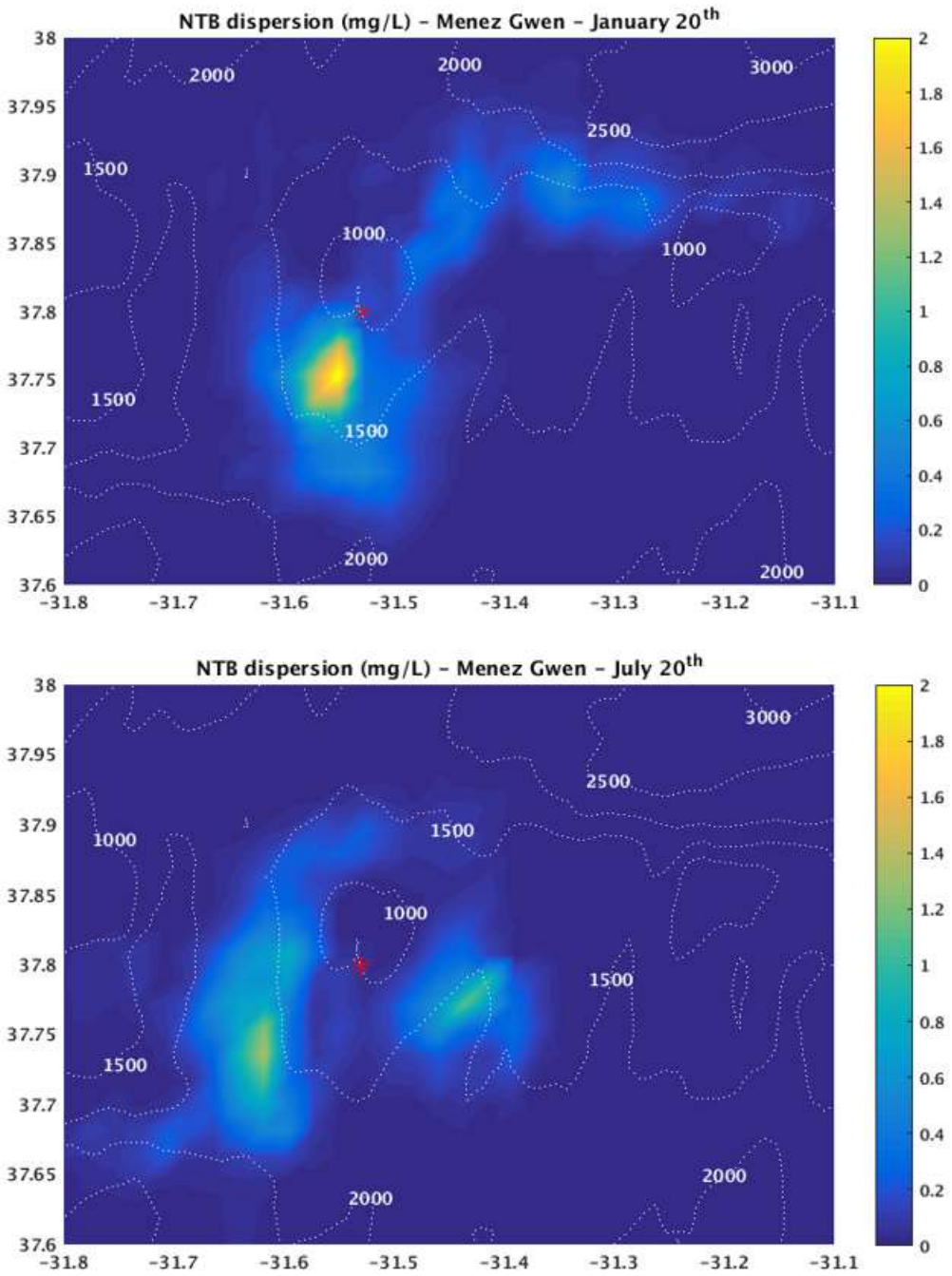

Figure 11. Settled final position of the Nitrobenzene around the MG hydrothermal vent, during the months of January (upper panel) and July (lower panel)

The dispersion and settling of PCE were similar to the ones observed for NTB, with the difference that a higher concentration was observed close to the MG (Figure 12). This can be due to the higher density of this HNS which also directly affects the settling velocity.

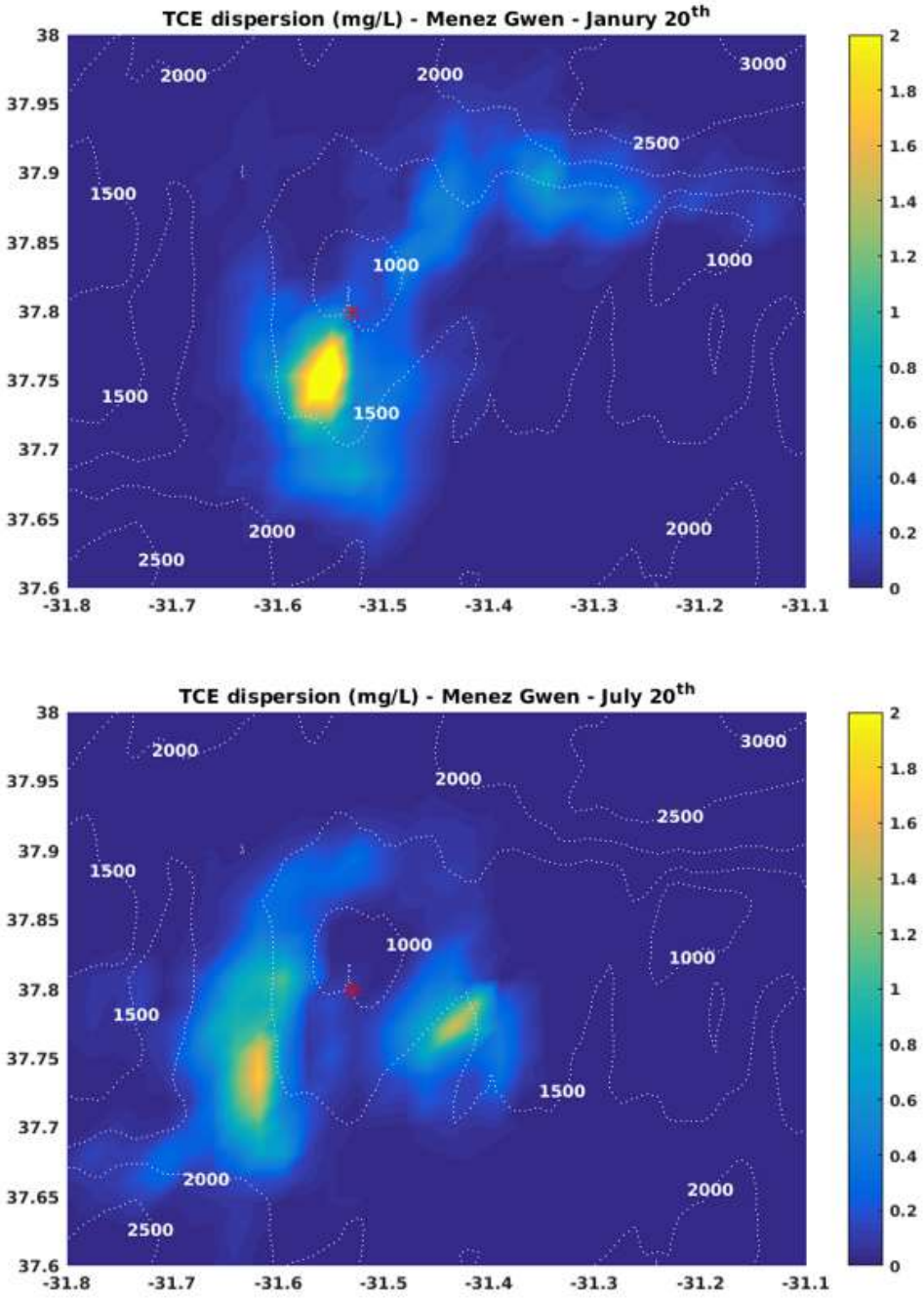

Figure 12. Settled final position of the Tetrachloroethylene around the MG hydrothermal vent, during the months of January (upper panel) and July (lower panel)

3.1.2.2. HNS dispersion – Seamount 10 (S10)

The hourly concentration of HNS over the S10 summit (Figure 13) showed a different behaviour than that observed at the MG. The seamount is located at a shallower depth, where local currents tend to be more intense which contributes to a faster dispersion of the droplets. Higher concentrations over the S10 summit for the

four HNS, were observed during January. The final position of the PCE and NTB droplets at the seafloor during January (Figure 14 and Figure 15) showed a circular behaviour around the S10 region, with lower concentrations than those observed during July, due to their persistency around the S10 summit (Figure 14 and Figure 15). For this month, the droplets showed a tendency to settle down at the NW region of the seamount area, which again is in line with the good representation of the local circulation features by the oceanic model and the assimilation of this behaviour by the semi-Lagrangian model.

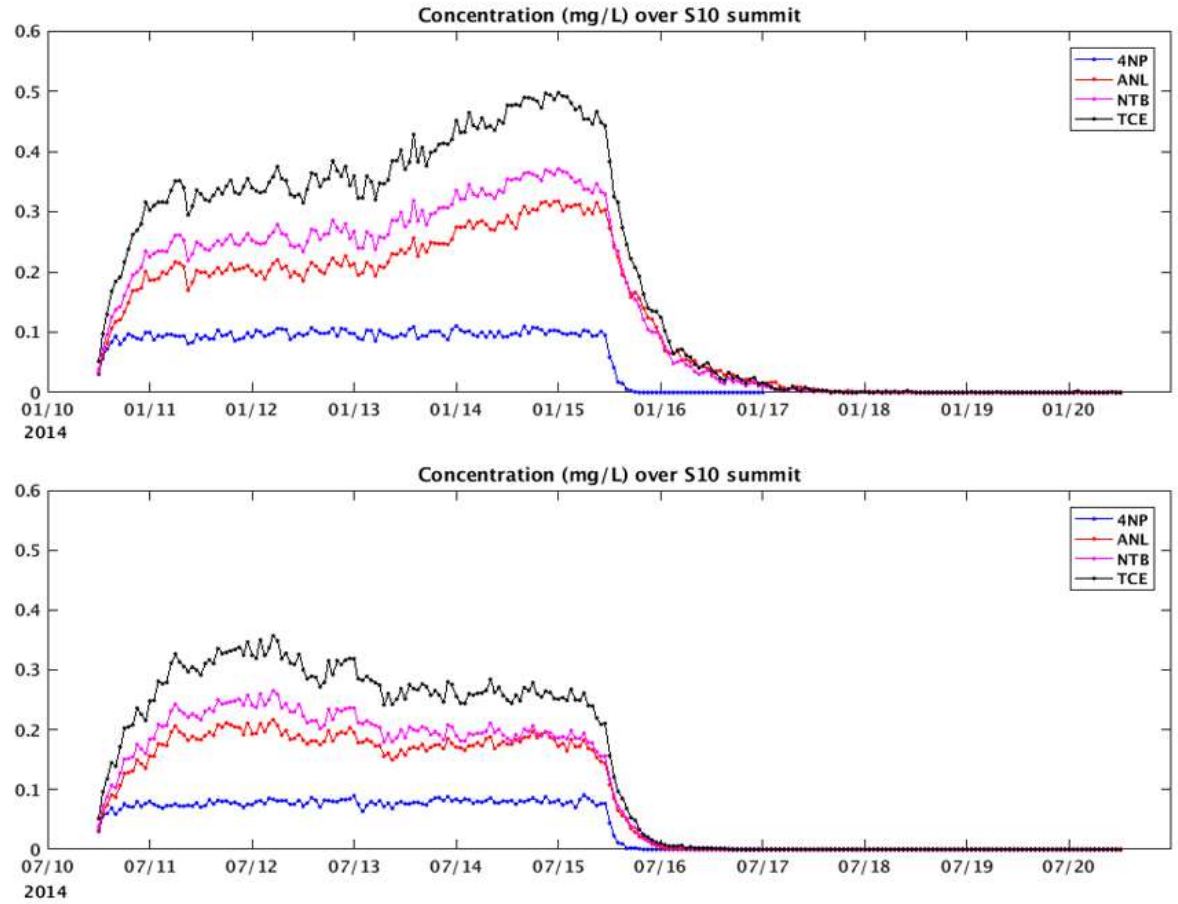

Figure 13. Hourly concentration of the selected HNS, over the S10 summit, during the months of January (upper panel) and July (lower panel)

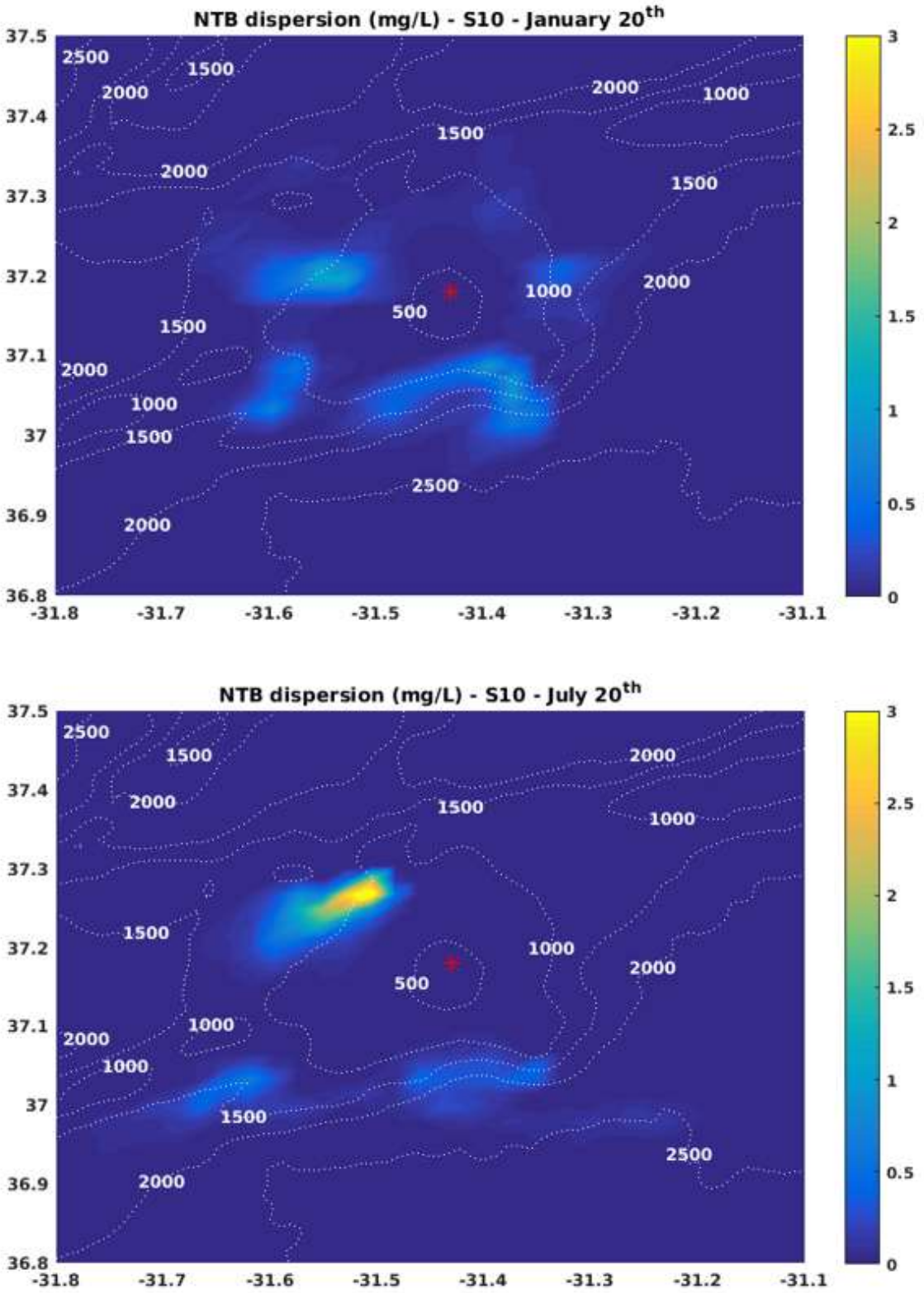

Figure 14. Settled final position of the Nitrobenzene around the S10 Seamount, during the months of January (upper panel) and July (lower panel)

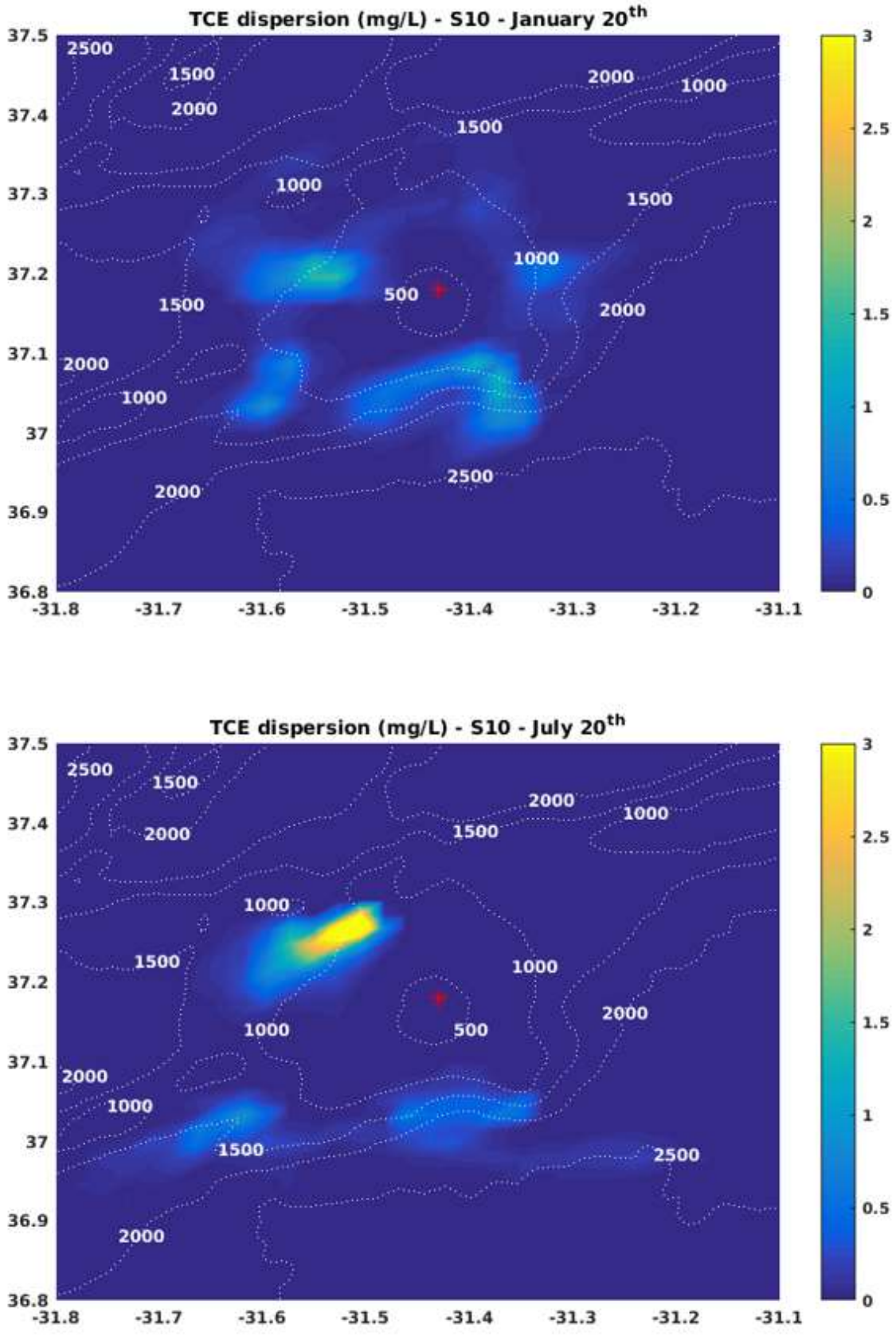

Figure 15. Settled final position of the Tetrachloroethylene around the S10 Seamount, during the months of January (upper panel) and July (lower panel)

3.2. AQUATOX Model

3.2.1. Seamount food web model (AQUATOX)

3.2.1.1. Abiotic data

The modelled abiotic data in AQUATOX (i.e., water temperature, salinity and nutrient concentration, such as nitrate, phosphate and dissolved oxygen) were compared against reference data (Figure 16).

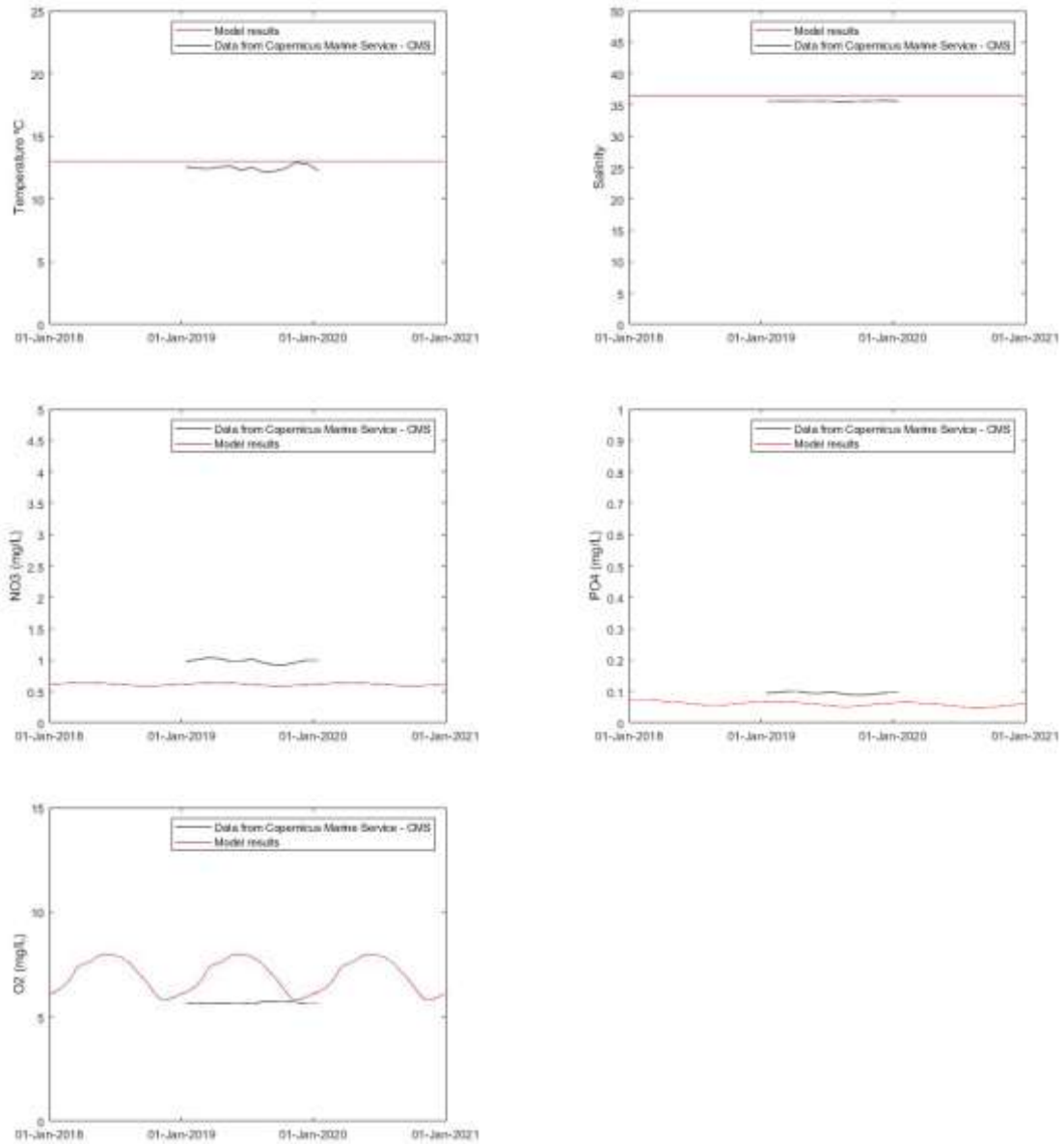

Figure 16. Comparison of the modelled abiotic data against reference data

Generally, the model results are consistent with the patterns of the natural system. Water temperature and salinity are well represented by the model, with slight overestimations of the model (red lines). However, for the nutrients (nitrate and phosphate), the model results clearly underestimate the reference data, which is most notorious for nitrate. However, for dissolved oxygen, the model presents seasonal variation, whereas in the reference data these oscillations are much less evident.

3.2.1.2. Biotic data

According to simulations, the seamount 10 ecosystem has an average GPP (Gross Primary Production) of 42 $gO_2\ m^{-2}\ d^{-1}$, with a P/R (production to respiration ratio) of 0.88 and a turnover (B/P- biomass to production ratio) of 3.3 days. The groups with higher production were large zooplankton, small zooplankton and shrimps (range: 1430-4822 g $m^{-2}\ y^{-1}$). Conversely, the production values of crabs, other benthos and habitat forming benthos were comparatively lower (range: $1.91E^{-6}$ - $1.94E^{-4}$ g $m^{-2}\ y^{-1}$). From the fish groups, mesopelagic fish had the highest production (2.09 g $m^{-2}\ y^{-1}$), whereas pelagic sharks the lowest (0.04 g $m^{-2}\ y^{-1}$).

The biomass variation of the functional groups throughout three consecutive years is represented in Figure 17. Compared to previous results obtained through EwE models [49], phytoplankton and some invertebrates (shrimp, habitat forming benthos, other benthos) are the worst represented species, with absolute errors of about 45%. The best represented invertebrate groups are small and large zooplankton and crabs with absolute errors below 10%. Conversely, fishes are the best represented groups, as the absolute error is always below 10%.

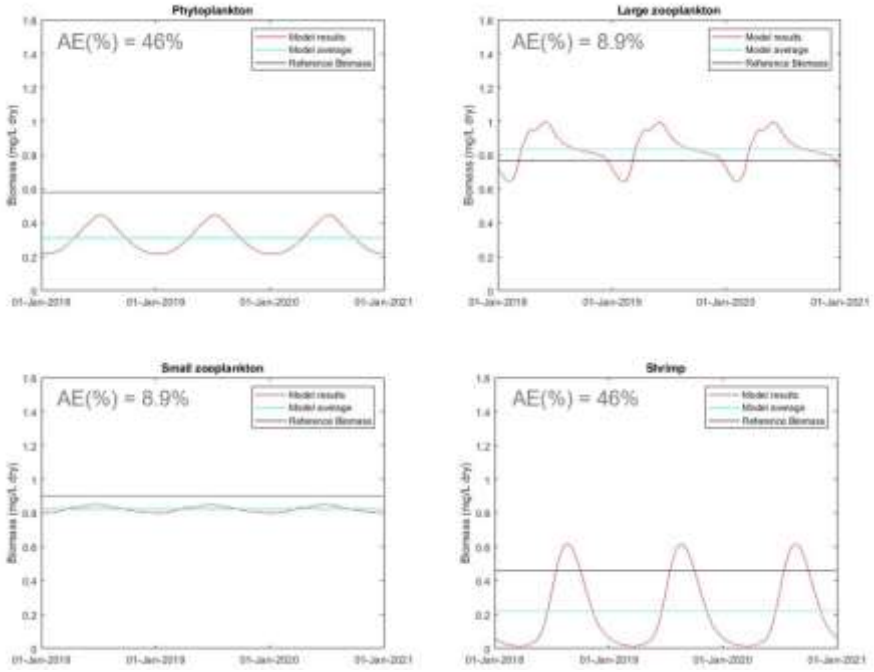

Figure 17. Comparison of modelled biotic data (biomass) against reference data (previously modelled)*, with respective absolute error*

(continuation of Figure 17)

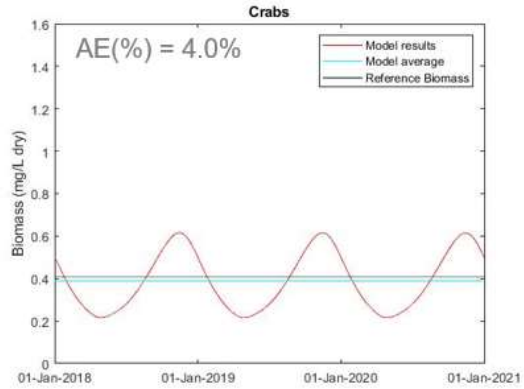

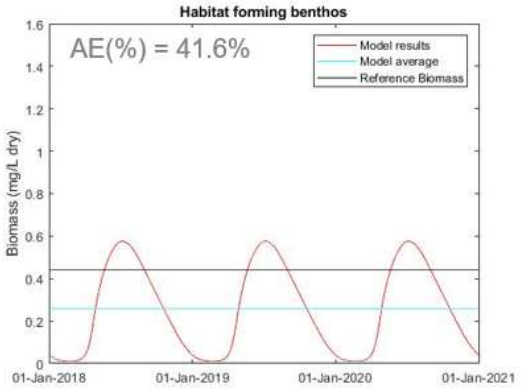

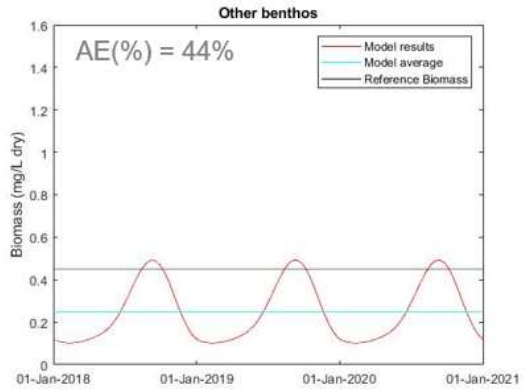

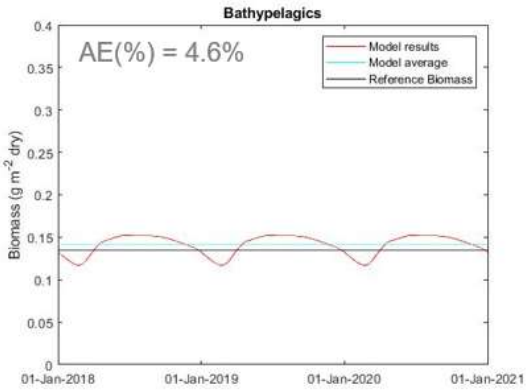

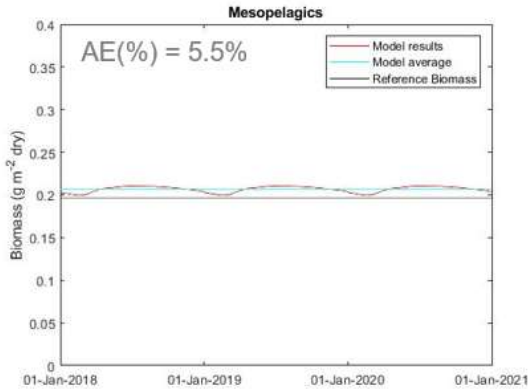

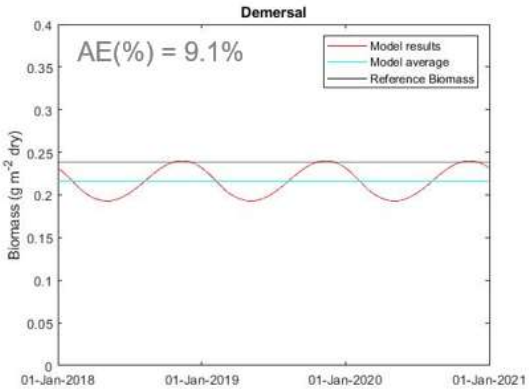

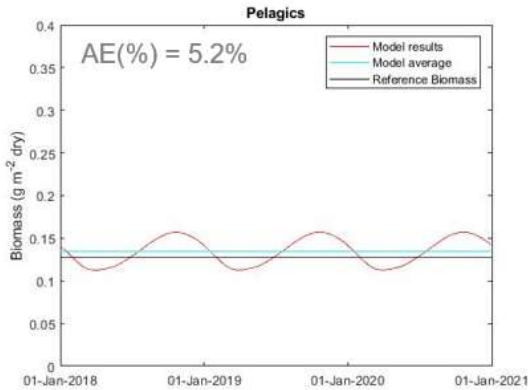

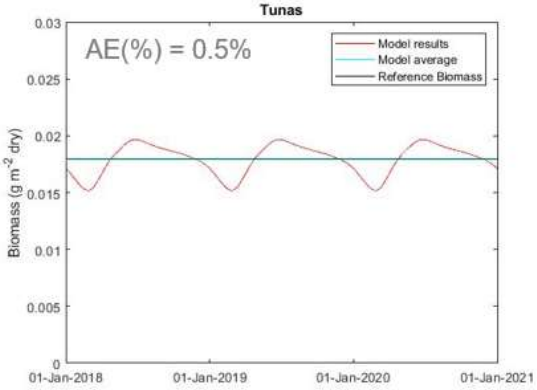

(continuation of Figure 17)

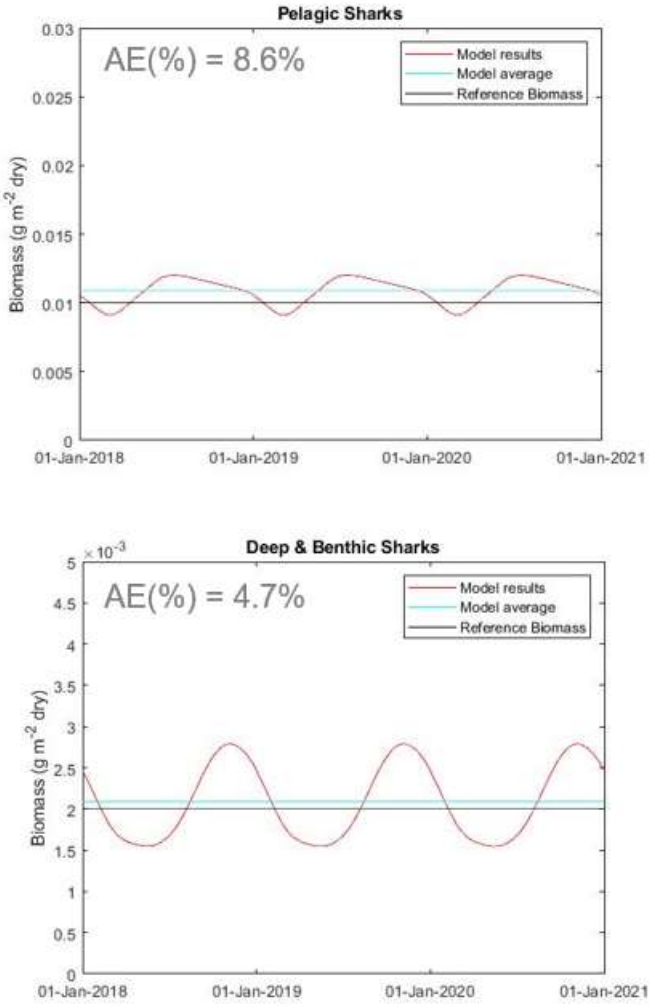

3.2.2. Sensitivity analysis

The sensitivity analysis for the functional groups included in the seamount model is represented in Figure 18. Although most of the functional groups present an expected variation of the state variable following a ±10% parameter variation (from 0 to 40%), some present exceptional high values. This is the case of shrimps (for the parameter minimum prey for feeding), where the sensitivity surpasses a 150% of variation in shrimp biomass for a single -10% variation. A similar pattern is also observed for pelagic fish (maximum consumption and maximum velocity).

We have also assessed the most sensitive parameters common to multiple functional groups (Figure 19). The results revealed that “Specific dynamic action” is the most sensitivity-inducing parameter, which is related to metabolic cost of digesting and assimilating prey (13 out of 14 groups), followed by optimal temperature and the carrying capacity of the system.

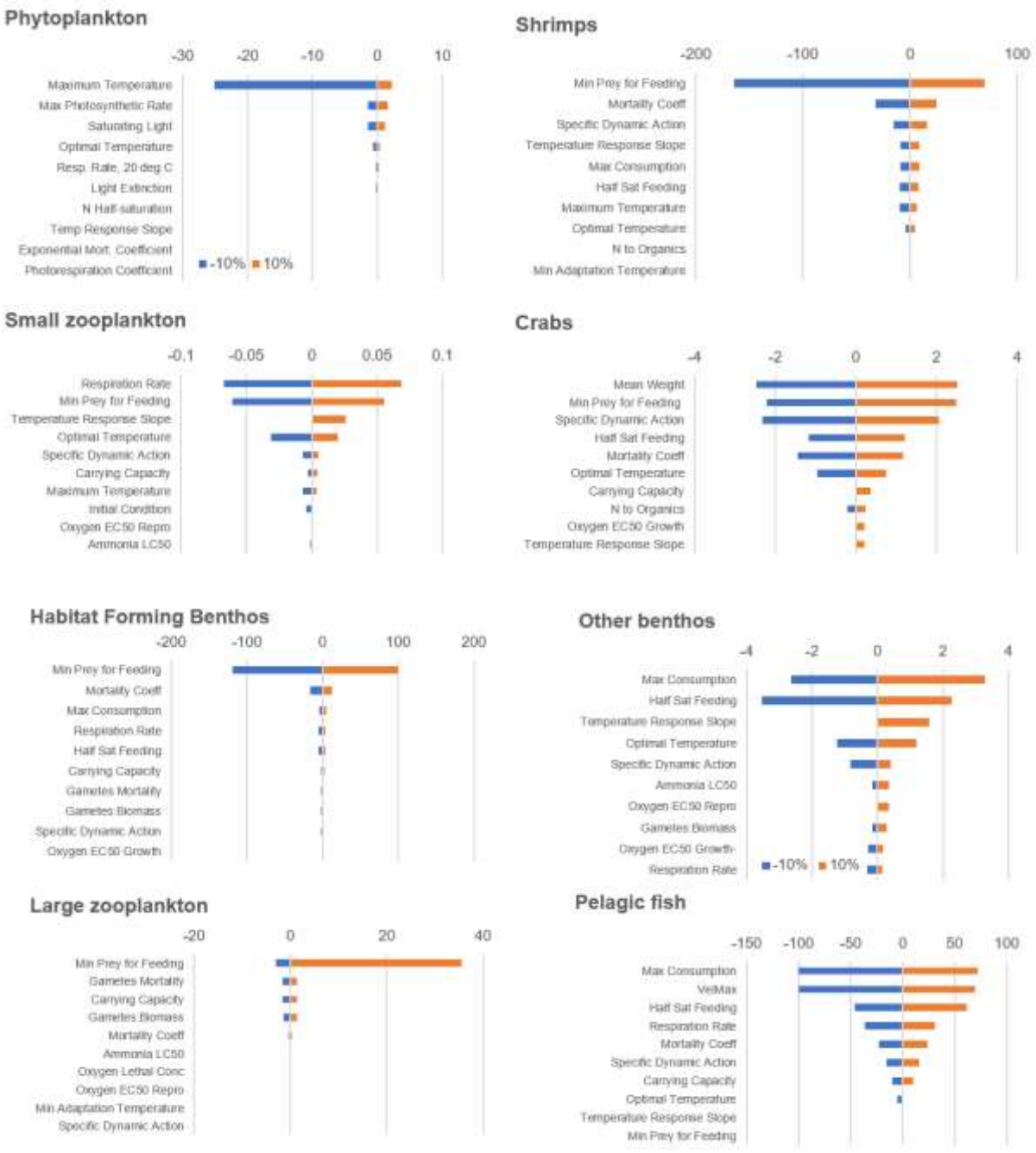

Figure 18. Sensitivity analysis for the top-10 most sensitive parameters for the biomass of the functional groups (biomass)

(continuation of Figure 18)

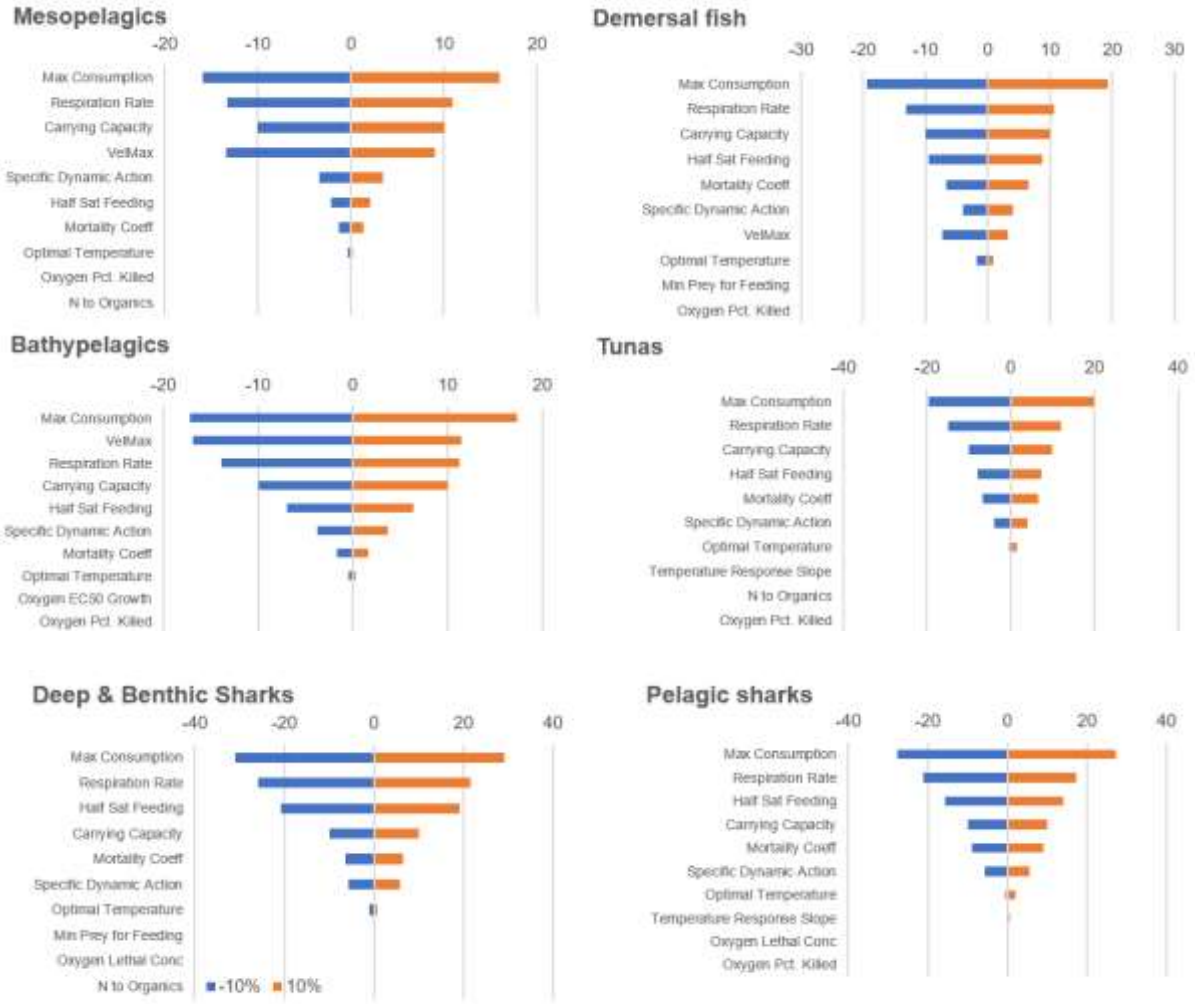

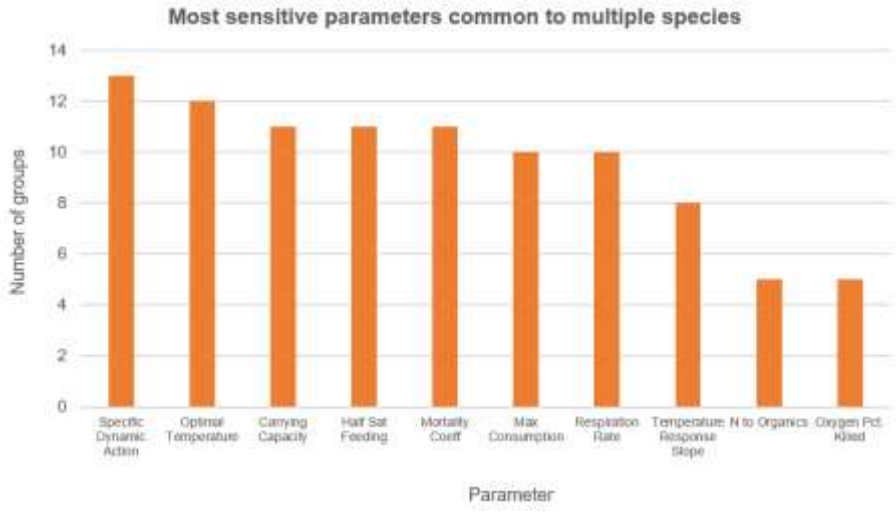

Figure 19. Most sensitive parameters common to multiple species

3.2.3. HNS effects on the seamount food web

Regarding the HNS effects in the seamount trophic web, they were only evaluated in terms of acute mortality (LC_{50}) due to the lack of available data for other ecotoxicological parameters.

We only present the results for the worst-case scenario, which for seamount S10 corresponded to the winter simulations. The most sensitive functional group was large zooplankton, that presented LC_{50} concentrations below the outputted concentrations from the Lagrangian model, for all HNS (cf. Table 5). Another group, the Habitat forming benthos, was sensitive to nitrobenzene and tetrachloroethylene (i.e., LC_{50} below the maximum concentration calculated at the seamount summit from the Lagrangian model) (cf. Table 5).

The model results deviated from our expectations, as we initially anticipated a more pronounced impact from sinkers, specifically nitrobenzene and tetrachloroethylene, leading to a lengthier recovery period for the system. However, our in-depth analysis of the model outputs revealed that dissolved oxygen decreases as a result of HNS breakdown, thereby indirectly affecting the dynamics of species.

Figure 20 shows the results for HNS simulations. We represent the expected trophic cascade effect, and the variation in the dissolved oxygen throughout the simulation.

The results suggest that in the event of an accidental spill, the system takes approximately 7 years to recover from aniline, followed by a 5-year recovery period for the sinkers (nitrobenzene and tetrachloroethylene), and ultimately a full system recovery after 3 years for 4-nonylphenol. These findings underscore the high complexity of the system, characterised by intricate feedback mechanisms predominantly driven by variations in oxygen levels.

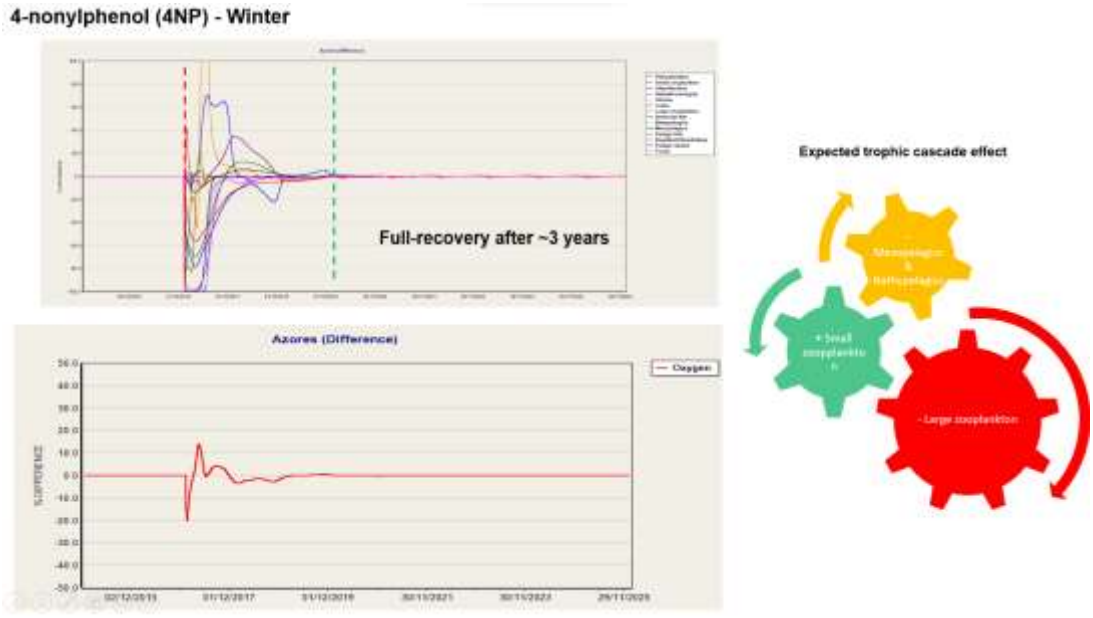

Figure 20. Results for HNS simulation in AQUATOX for seamount trophic web (upper panel), variation of dissolved oxygen (lower panel) and expected trophic cascade effect (right panel)

(continuation of Figure 20)

Aniline (AN) - Winter

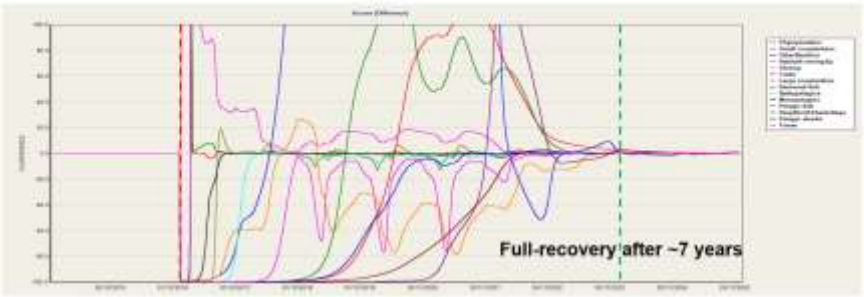

Nitrobenzene (NB) - Winter

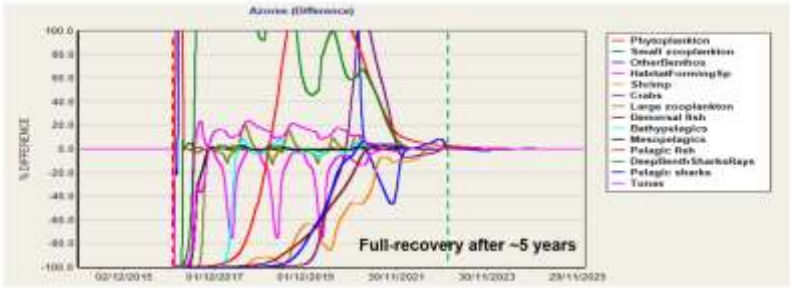

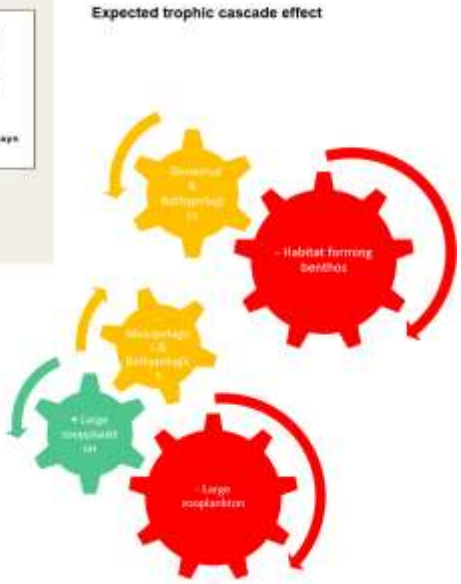

(continuation of Figure 20)

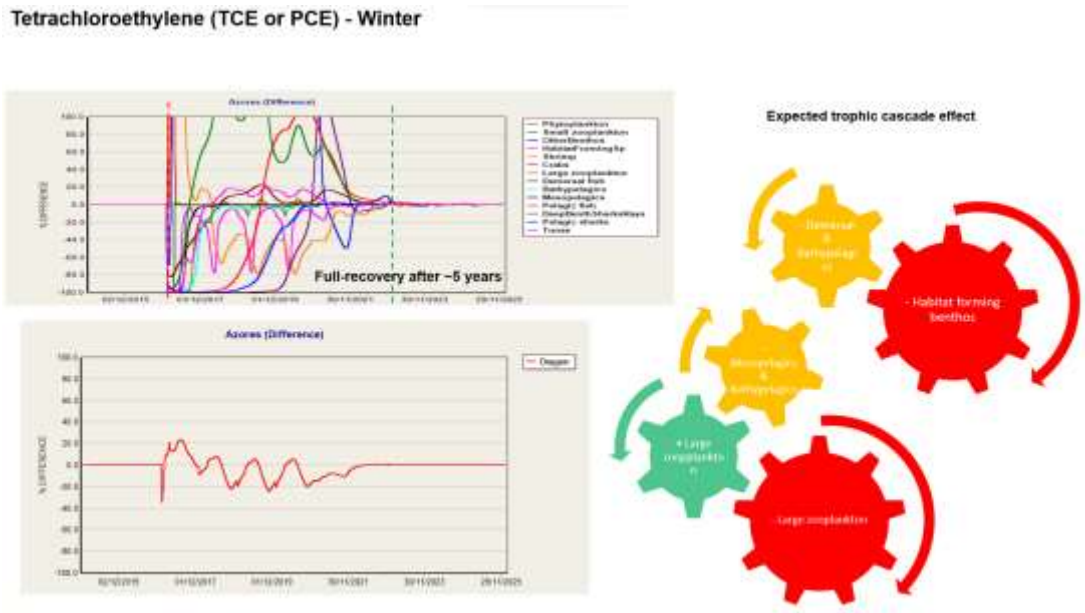

3.3. Ecopath with Ecosim Model

3.3.1. Menez Gwen food web model

The MG Ecopath model consists of three trophic levels (Figure 21). The input and output parameters for each functional group (FG) of the MG-Ecopath model are presented in the Table 9. "Vent Mussels" dominate in terms of biomass, representing 84% of the total biomass, although contributing with only 4% to total consumption. "Copepods" have the largest proportion of total consumption (45%) despite having the lowest omnivory index, while "vent Crabs" have the highest omnivory index (0.33) as top predators. Most consumer groups have Ecotrophic Efficiency (EE) values ranging from 0.307 to 0.56, except for detritus groups with lower EE values. The model's vital rates and trophic relationships are physiologically realistic, indicating its consistency and coherence.

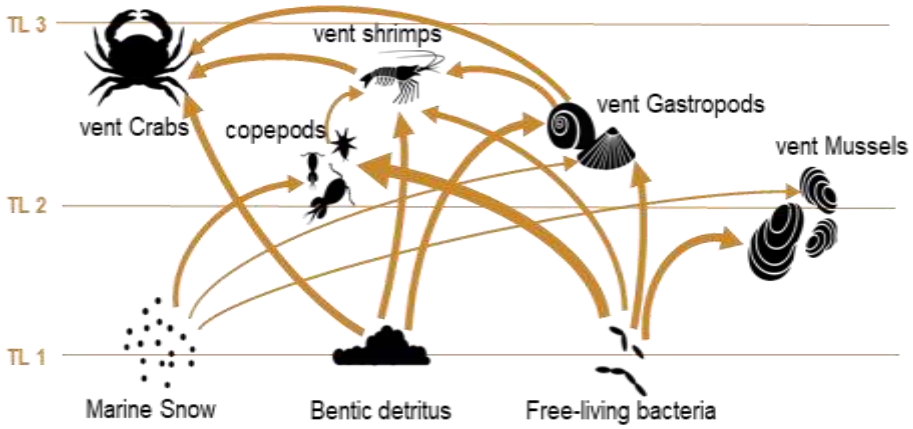

Figure 21. Ecopath flow diagram of the MG food web model, at MAR. TL: Trophic Level; The arrows indicate feeding relationships, and line width indicates the proportion of the diet composition transferred to other TLs

Table 9. Input and output (in bold) parameters for each functional group (FG) of the MG Ecopath model

	FG	TL	B	P/B	Q/B	EE	OI	KS
1	vent Crabs	2.506	2.602	0.316	1.764	**0.000**	**0.330**	**-0.033**
2	vent Shrimps	2.326	2.503	0.764	3.921	**0.216**	**0.249**	**-0.327**
3	vent Gastropods	2.105	12.022	1.228	5.435	**0.242**	**0.100**	**-0.676**
4	Copepods	2.053	17.637	2.585	10.305	**0.364**	**0.053**	**-1.138**
5	vent Mussels	2.000	1520.218	0.246	1.037	**0.000**	**0.125**	**-1.664**
7	Free-living bacteria	1.000	**17.812**	181.069	--	0.290		**-0.316**
8	Marine Snow	1.000	131.454	--	--	**0.094**		**--**
9	Benthic detritus	1.000	100.000	--	--	**0.010**		**--**

TL: trophic level, B: Biomass ($t.km^{-2}$), P/B: Production/Biomass (y^{-1}), Q/B: Consumption/Biomass (y^{-1}), EE: Ecotrophic Efficiency, OI: Omnivory Index, KS: Keystoneness index

The Mixed Trophic Impact (MTI) analysis (Figure 22) revealed that "Free-living bacteria" and "vent Mussels" have the greatest impacts on a larger number of groups within the community. On the other hand, "vent Crabs" had the greatest negative impact on their prey, specifically, on "vent Shrimp." Based on the Keystoneness Species index (KS) given by the Ecopath model, “vent Crabs" and "Free-living bacteria" are key species in the MG system (KS = -0.033 and KS = -0.316, respectively, Table 9).

The pattern of energy and biomass flow in the MG system, depicted by the Lindeman spine plot (Figure 23), revealed that the primary producers (P) account for approximately 18% of the total system throughput, despite representing only 1% of the living biomass.

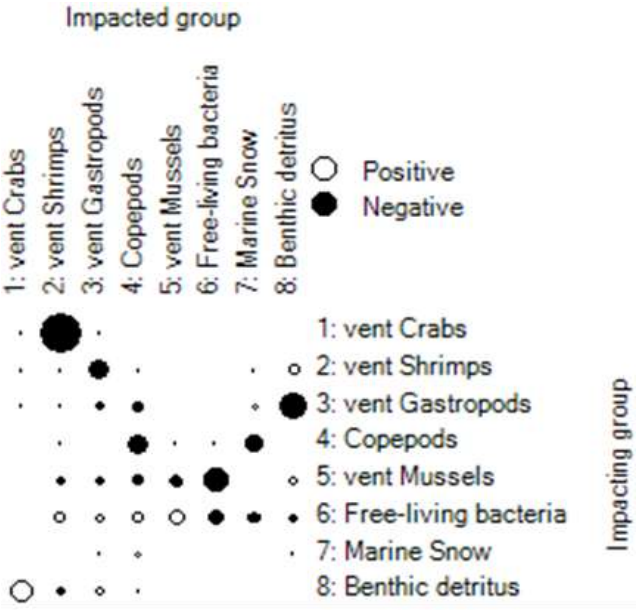

Figure 22. Mixed trophic impact matrix of each functional group on the other groups in the model

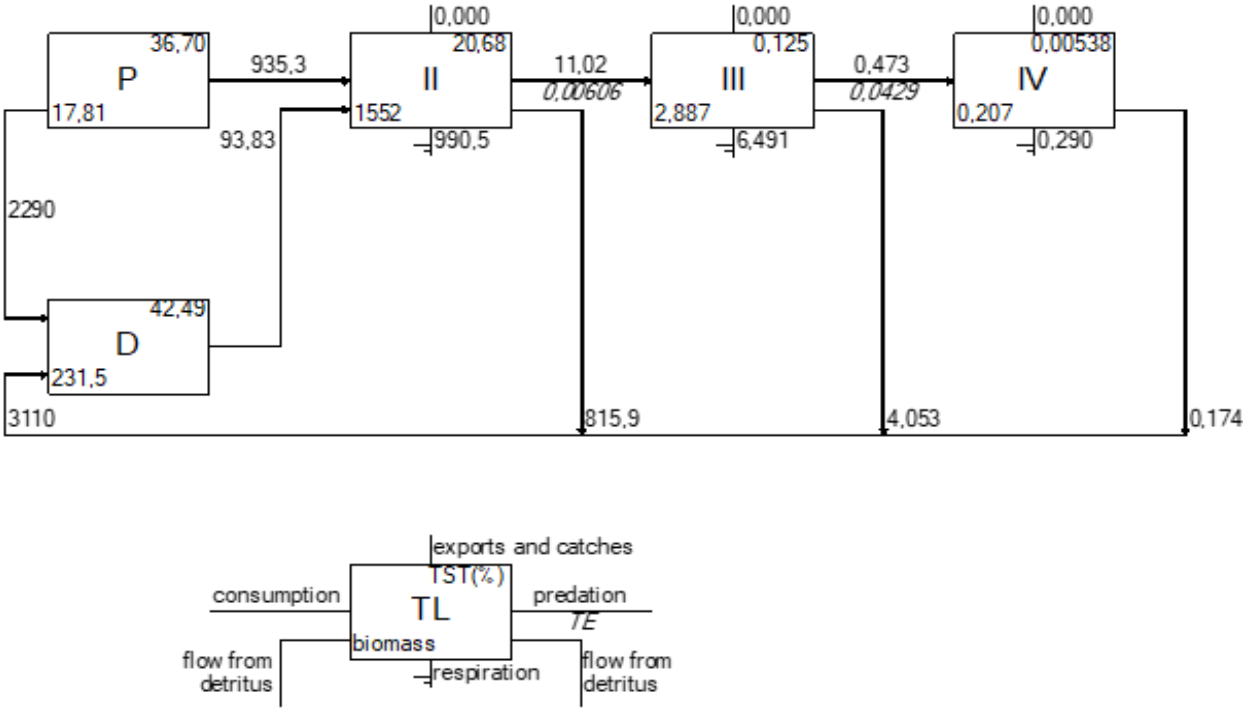

Figure 23. Lindeman spine plot of energy flows and biomasses, aggregated by discrete trophic levels

The TL II group, which includes the dominant species "vent mussels," showed higher respiration values and had the highest contribution to the detritus group. Contrary to the expected pattern described by [74], transfer efficiencies (TE) did not decrease with increasing Trophic Level (TL). In fact, the TE from TL II was lower than that from TL III. This unexpected pattern may be attributed to the features of the foundation species in the MG community, the "vent Mussels." As a foundation species, "vent Mussels" are not directly preyed upon by any other functional group [75] and, thus, do not contribute to the energy transfer to the subsequent trophic level, despite their substantial biomass.

Overall, the model results show that the MG food web exhibits a high exchange rate of energy and matter, with notable flows reported for respiration (997.26 $t.km^{-2}.y^{-1}$), export (3 016.17 $t.km^{-2}.y^{-1}$), detritus (3 733.53 $t.km^{-2}.y^{-1}$), consumption (1 837.96 $t.km^{-2}.y^{-1}$), production (3 661.95 $t.km^{-2}.y^{-1}$), and the total system throughput (9 584.91 $t.km^{-2}.y^{-1}$) (Table 10). The total biomass (excluding detritus) is 1 572.79 $t.km^{-2}$, and the total net primary production is 2 227.93 $t.km^{-2}.y^{-1}$, which closely align with previous studies at hydrothermal vent systems (Total Biomass = [2 000 - 8 500] $t.km^{-2}$ in [62] and Production = [380 - 9 300] t $C.km^{-2}.y^{-1}$ in [63]). Ratios between flows, such as total primary production/total respiration (TPP/TR = 3.2), total primary production/total biomass (TPP/TB = 2.05), and total biomass/total throughput (TB/TST = 0.16), indicate lower accumulation of heterotrophic biomass. However, total transfer efficiency (TE = 1.64%) and Finn's Cycling Index (FCI = 0.22%) are low, suggesting inefficiency in energy use. The Connectance Index (CI = 0.44) and System Omnivory Index (SOI = 0.11) also indicate a low number of feeding interactions. Ascendancy (A = 46%) and Overhead (O = 54%) reflect moderate values for ecosystem development and resilience, respectively. The model's Pedigree index (0.455) falls within the reliable range of data quality, suggesting that the model was constructed using a reliable quality of source data [76].

Table 10. Ecosystem attributes revealed by the MG Ecopath model

Parameter	Value	units
Sum of all consumption	1 837.96	$t.km^{-2}.y^{-1}$
Sum of all exports	3 016.17	$t.km^{-2}.y^{-1}$
Sum of all respiratory flows	997.26	$t.km^{-2}.y^{-1}$
Sum of all flows into detritus	3 733.53	$t.km^{-2}.y^{-1}$
Total system throughput (TST)	9 584.91	$t.km^{-2}.y^{-1}$
Sum of all production	3 661.95	$t.km^{-2}.y^{-1}$
Calculated total net primary production	3 225.19	$t.km^{-2}.y^{-1}$

(continuation of Table 10)

Parameter	Value	units
Total primary production/total respiration (TPP/TR)	3.23	$t.km^{-2}.y^{-1}$
Net system production	2 227.93	$t.km^{-2}.y^{-1}$
Total primary production/total biomass (TPP/TB)	2.05	$t.km^{-2}.y^{-1}$
Total biomass/total throughput (TB/TST)	0.16	$t.km^{-2}.y^{-1}$
Total biomass (excluding detritus)	1 572.79	$t.km^{-2}$
Connectance Index (CI)	0.44	
System Omnivory Index (SOI)	0.11	
Ascendency (A)	46	%
Overhead (O)	54	%
Finn's cycling index (FCI)	0.22	% of TST
Ecopath pedigree	0.455	
Shannon diversity index	0.19	$t.km^{-2}.y^{-1}$
Development Capacity (C)	29 471.00	flow bits
Transfer efficiencies (TE)	1.66	%

3.3.2. HNS effects on the Menez Gwen food web

Among the two groups directly impacted by the tetrachloroethylene (PCE) spill, the “vent Gastropods" showed the most rapid recovery in terms of biomass. Within two years after the incident (year 4), their biomass returned to pre-incident levels and even exceeded the initial values, reaching a maximum increase of approximately 17%, five years after the incident (year 6) (Figure 24). After this maximum, the decreasing trend remained until it reached values very close to the initial ones.

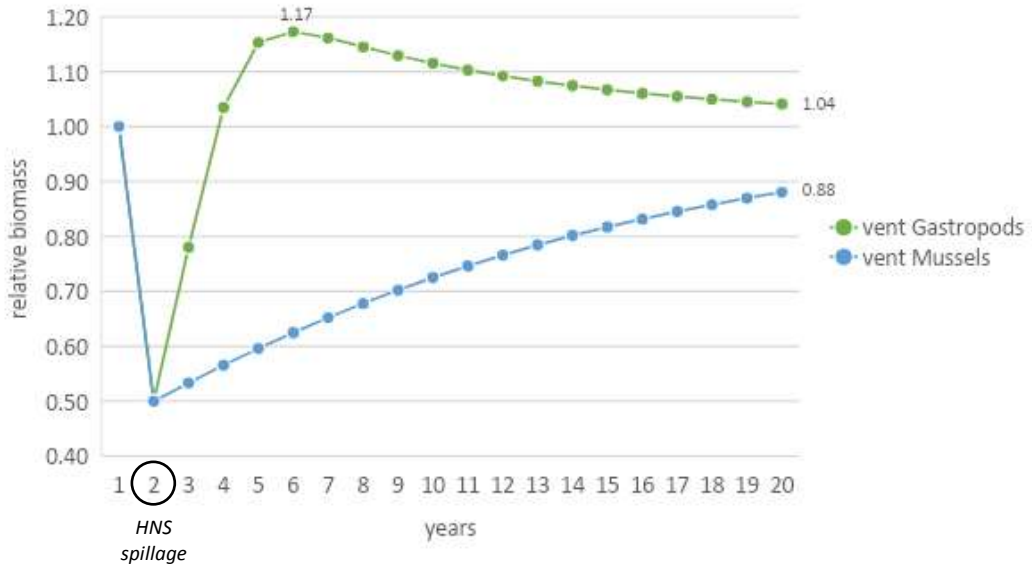

Figure 24. Variation of the biomass of the groups directly affected by the PCE spill: "vent Gastropods" and "vent Mussels". The circled year 2 represents the year in which the hypothetical PCE Spill occurred (i.e., when the Forcing Functions (FF 50) are applied, to these two groups, causing a reduction of 50% in their biomasses

In the case of "vent Mussels," they experienced a stronger biomass reduction caused by the PCE spill, leading to a slower recovery. Even after a period of eighteen years following the incident, their biomass values remained below the initial values, with a reduction of approximately 12% compared to the beginning of the simulation (Figure 24).

The reduction of biomass in the two groups affected by the PCE spill led to a slight increase of the initial biomass of the highest TL groups (+1% for “vent Crabs” and +2% for “vent Shrimps”), during the year of the accident, followed by a decreasing trend in the following years, with "vent Crabs" being the most affected, with a marked decline. Nonetheless, over time both groups gradually recovered and their biomasses reached values slightly above those verified before the incident. For "vent Shrimps", the recovery occurred less than 2 years after the spill, while "vent Crabs" required 5 years to recover (Figure 25).

Contrarily, the remaining groups, detritus ("Marine Snow" and "Benthic detritus"), primary producers ("free-living bacteria"), and consumers ("Copepods"), exhibited an increase in their biomasses as a result of the spill, with "Copepods" showing the highest increase, reaching up to approximately 30% above the initial biomass. However, the initial increasing pattern gradually declined over the simulation period, eventually converging towards values close to the pre-incident period (Figure 26).

Overall, by the end of the 20-years simulation, all groups showed biomass values similar to pre-incident values (Figure 27).

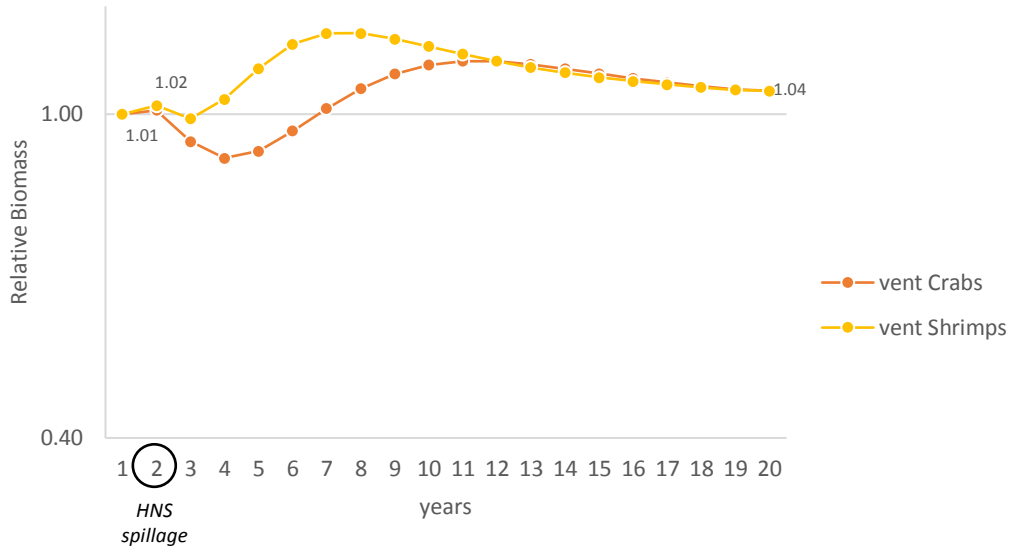

Figure 25. Biomass variation for the groups "vent Crabs" and "vent Shrimps" throughout the simulation period. The circled year 2 represents the year in which the HNS (PCE) spill occurred

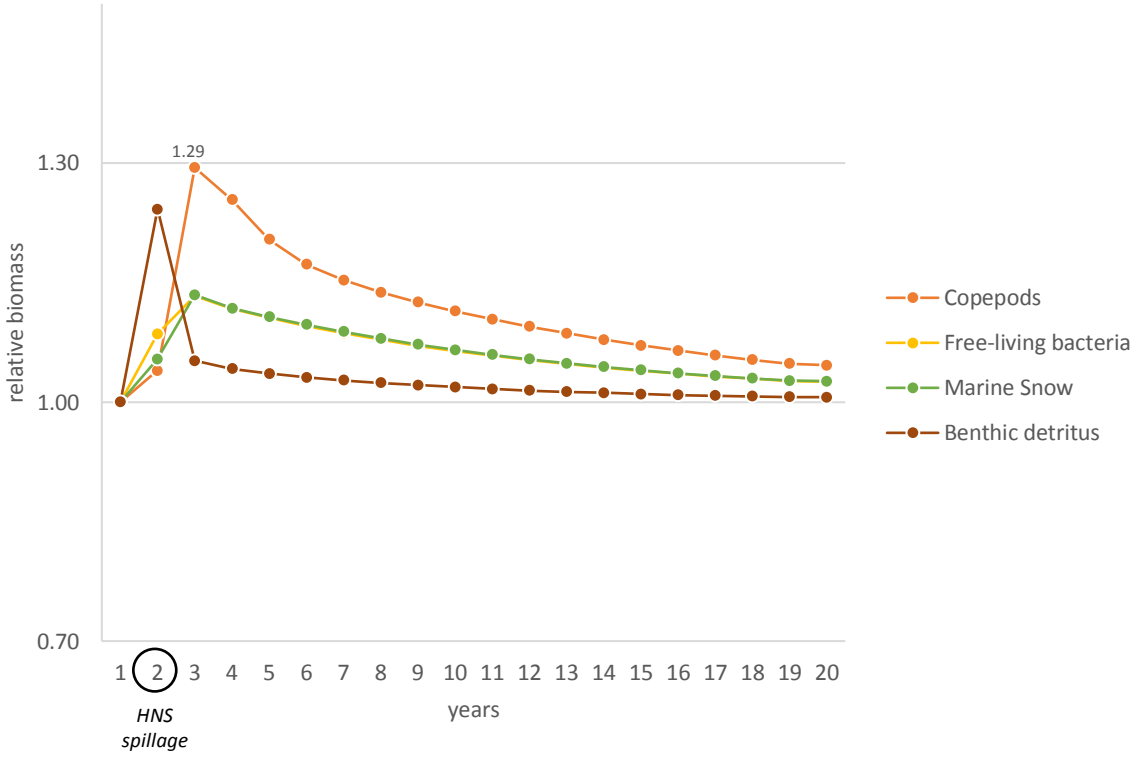

Figure 26. Biomass variation of the following groups: "Marine Snow," "Benthic detritus," "free-living bacteria" and "Copepods" during the simulation period. The circled year 2 represents the year in which the HNS (PCE) spill occurred

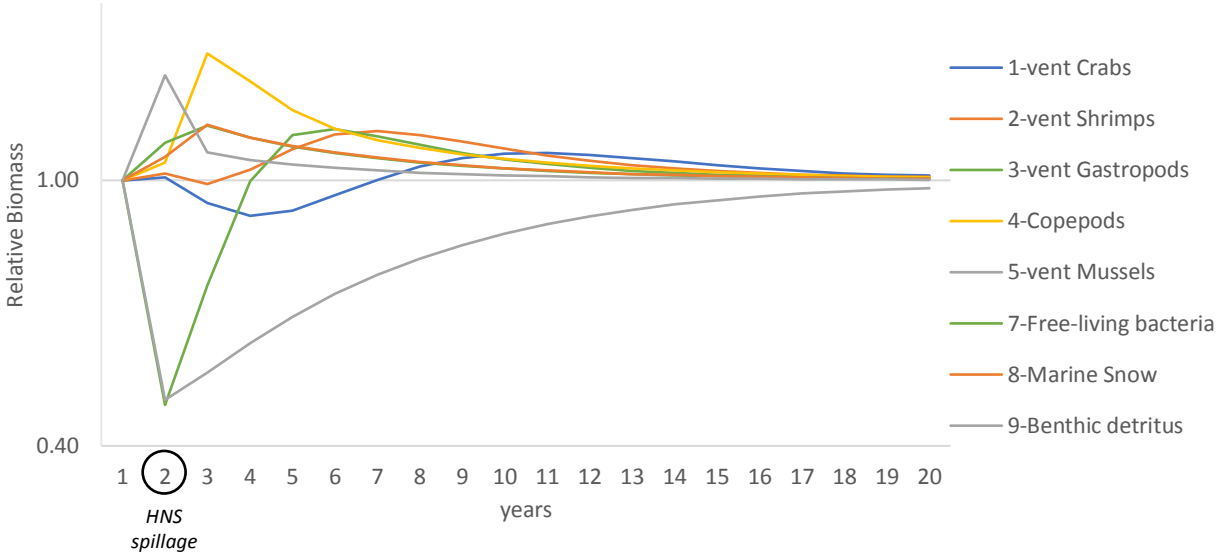

Figure 27. Biomass variation of functional groups of the MG community during the simulation of the PCE spill. The circled year 2 represents the year in which the HNS (PCE) spill occurred

4. DISCUSSION

4.1. Ocean circulation and Lagrangian models

The configuration adopted for the ocean numerical modelling was able to reproduce the local circulation and features, covering the representation of the submesoscale processes (1-10 km) related to instabilities promoted by topographic constraints. The model resolution (1 km) and parameterization were able to account for the turbulent mixing processes which affects the HNS behaviour close to the sites considered and on the seafloor. We represented the processes at the second phase of a seafloor spill, and weathering processes were not included, which is in line with the assumption adopted for most oil spill models (e.g., GNOME, HNS-MS). Nonetheless, dissolution of HNS should be considered for the characterization of the long-term impact on marine fauna.

4.1.1. Limitations of the ocean circulation and Lagrangian models

As previously mentioned, the OpenDrift model does not consider the weathering processes of particles, which constitutes a limitation for a realistic representation of contaminants, such as HNS. In fact, depending on the surrounding conditions of temperature and pressure, HNS may change their behaviour and, thus, their effects on biota may also change substantially.

In the future, this limitation may be overcome by the numerical representation of all relevant weathering and chemical processes (e.g., evaporation, oxidation, biodegradation) of the HNS particles in the script of the implemented semi-Lagrangian tool.

4.2. Seamount 10 ecosystem model

To develop the seamount ecosystem model, we used AQUATOX software. The model results for abiotic parameters such as the water temperature and salinity were very well represented. However, nutrients, especially nitrate, were underestimated, possibly due to the fact that our reference data considers upwelling and, therefore, accounts for nutrient enriched waters rising to more superficial ocean layers. Future improvements should include a time-series as input of nutrients resulting from upwelling into the model to improve it.

Conversely, modelled dissolved oxygen presented more pronounced seasonal patterns and was overestimated in relation to reference data, indicating that probably the nitrification process is underestimated in the model, as there is less nitrate and more dissolved oxygen than the expected [77].

Comparisons of the seamount functional groups' results with other data are limited due to: i) the lack of observed or estimated data for Atlantic seamount food webs, and ii) the data available result from different models with different structures and assumptions.

Nevertheless, taking into consideration the absolute error estimation, the present results were more promising for the functional groups of fishes (Pelagic Fish, Demersal Fish, Mesopelagic fish, Tunas, Bathypelagic Fish, Pelagic Sharks, Deep and benthic sharks and rays). This may be due to a better parameterization of these groups, as parameters like growth rates, consumption rates, and mortality rates, might be better tuned or calibrated for fishes, leading to lower errors for those species. In fact, there are comprehensive works on these groups for the study area, which supported their parameterization [4, 5]. Other potential explanations for this outcome may be related to low trophic species involved in more intricate and interconnected trophic interactions, making it more challenging to accurately model the dynamics of primary producers and their consumers. Therefore, and foreseeing the potential enhancement of the model's performance, we suggest further data sampling and gathering to improve the accuracy, seasonality and representativeness of data used for parameterizing the model, especially for lower trophic species.

Previous works regarding seamount food web models are scarce [49, 78] and use another model software (e.g., EwE), which considers different assumptions and model outputs. When comparing total biomass (excluding detritus), our results reveal a lower biomass (3.83 t DW km^{-2} or 19.15 t WW km^{-2}, if considering a FW to DW ratio of 5 - AQUATOX default) than those reported for the Azores EEZ (24.73 t WW km^{-2}, [49]). However, in deep-sea systems of the Catalan margin (Spain) and Southern Plateau (New Zealand), the total biomass (excluding detritus) are closer to those obtained in this work (3.93 and 6.22 t km^{-2}, respectively for [79] and [80]). Please note that, for [80], there is no mention whether the presented results are in dry or wet weight). The sum of all production for this work was 42.09 t km^{-2} y^{-1}, which contrasts with a substantially higher value presented for the Azores EEZ (1763.11 t km^{-2} y^{-1}, [49]) and slightly higher than those found for Catalan margin (14.83 t km^{-2} y^{-1}, [79]). Major differences between the referenced articles and this work may be due to the oversimplifications of the trophic web, by an aggregation of functional groups and diets. However, this was necessary as AQUATOX requires over 20 parameters for each species, most of them scarcely unknown for the majority of deep-sea species.

The results of sensitivity analysis complement this statement, as in some cases there were unexpectedly highly sensitive model parameters (e.g., minimum prey of feeding for Shrimps and Habitat Forming Benthos; maximum consumption for Pelagic Fish). These results can simply indicate a strong parameter influence, where certain input parameters have a large impact on the model output. However, we believe that due to the system complexity and consequent model complexity, the likely cause is not as such. Instead, it is possible that model simplification led to unrealistic assumptions that, consequently, overestimate the effects of certain parameters, ultimately resulting in high sensitivity. Moreover, the complexity of the model can underlie interactions or dependencies, including nonlinear relationships between input parameters and the model output, amplifying the effects of parameter changes, and also resulting in higher sensitivity values.

Despite the limitations of the seamount food web model (enumerated in the next section), we simulated the effects of HNS according to the maximum concentrations outputted by the circulation and lagrangian models at the seamount summit. Although we would expect worst ecological consequences, in terms of recovery time, for tetrachloroethylene (PCE) and nitrobenzene (NTB) due to their sinking behaviour, it was aniline (AN) that revealed the longest recovery period. This is probably related to specific physico-chemical parameters that highly influence the consequent breakdown in the system, with further consumption of dissolved oxygen that leads to anoxic conditions and further mortality.

In more detail, and regarding the 4 nonylphenol (4NP), the most affected functional groups were "Pelagic fish" and "Pelagic sharks", which is expected given the persistent floater behaviour of this HNS (i.e., it is expected to affect mostly pelagic groups). This result also suggests bioaccumulative and biomagnifying effects of 4NP throughout the food web, which is also consistent with previous studies for other marine species [81, 82].

For aniline (AN), the model results reveal that most species are negatively affected and take a relatively long time to recover, compared with the others HNS. The most affected functional groups are Shrimps, Crabs, Tunas, Pelagic Sharks, Pelagic Fish, Deep benthic sharks and rays, and Other Benthos. However, species that live in the dependency of the seafloor (i.e., benthic species) tend to present a faster recovery, such as the functional groups of Deep benthic sharks and rays and Other Benthos. The range of functional groups affected may be related to a longer breakdown in the system, while the fastest recovery of benthic groups may be related to the floater/dissolver behaviour of AN. In addition, note that, in the presence of light and oxygen, some freshwater microalgae are able to accelerate the photodegradation of aniline [83]. The high depths and low light conditions may not be favouring these degradation processes in seamounts, supporting the results found out in this work.

The results for nitrobenzene (NTB) and tetrachloroethylene (PCE) showed that the most affected functional groups are Shrimps, Crabs, Habitat Forming Benthos, Pelagic Fish and Pelagic Sharks. For NTB, the functional groups of Tunas and Deep benthic sharks and rays are also affected, but had a relatively fast recovery, when compared to other functional groups. Although we would expect that benthic species would be more affected, considering the sinker/dissolved behaviour of NTB and PCE, the results revealed that lower trophic groups (e.g., Shrimps and Crabs) presented a longer recovery period. Moreover, in the case of NTB and PCE, higher trophic functional groups (Pelagic Sharks and Pelagic Fish, respectively) presented a longer recovery time, suggesting a potential bioaccumulation, which is a consistent occurrence for other species [84].

In summary, the results of HNS exploratory scenarios pointed out that the functional groups of Shrimp, Crabs, Habitat Forming Benthos (represented in this seamount model by a sponge) and Pelagic sharks are the most sensitive species (i.e., take longer time to fully recover), to the most adverse HNS selected in this work (AN, NTB and PCE). These results suggest, together with the importance of these groups for higher trophic organisms and health of seamount trophic web, that future research directions should point for more extensive experimental and/or in situ assessments on their dynamics and life cycle traits. Moreover, these same functional groups are those that present higher sensitivity to model parameters, supporting the need of further good-quality datasets and model improvements.

4.2.1. Limitations of the Seamount 10 ecosystem model

Food webs are useful ways to consider the feeding structure of communities, illustrating feeding relationships. They comprise the basis of food web models, establishing major pathways of matter and energy flows. The approach followed in the present work represents a trade-off between food web complexity and representativity of a reference North Atlantic seamount, which constitutes a simplification of the natural system, as in every model [85]. As so, in the process of constructing the seamount food web, certain practical considerations required simplifications by aggregating some species and their corresponding dietary items.

While this approach facilitated and allowed the modelling process in AQUATOX (there is a maximum number of 16 functional groups of fish that can be accounted for in AQUATOX), it is important to acknowledge that such simplifications may inadvertently introduce artefacts into the food web. This can consequently lead to the formation of feeding links between functional groups that do not typically engage in such interactions. For instance, when multiple species are joined into a single group and share a common prey item, it can lead to artificial feeding relationships that would not occur in nature. Future improvements should aim to address these artefacts by incorporating more detailed data and refining the level of aggregation, to further enhance the accuracy and reliability of the models. Moreover, a close examination of the diet of each functional group, through field observations, fatty acids content and stable isotope analysis (SIA) or, in alternative, dissection of faeces or gut contents, are possible strategies to overcome this limitation. Although some of these techniques have been already addressed in the literature for seamounts [86-90], they do not include all the functional groups.

Food webs, and consequently the food web models, do not consider other relevant processes that occur in natural systems and affect the feeding and dietary relationships, such as other ecological aspects, including behaviour. In fact, the AQUATOX model (and other ecosystem models) simulate static webs, while real food webs are highly dynamic with feeding links appearing and disappearing or varying in strength. Species are known to meet their nutritional needs, for example, in response to the population dynamics of a potential prey [85]. This simplification can account for a relevant source of uncertainty in the model, as changes in biodiversity itself can lead to complex if predictable changes in ecosystem processes and, conversely, food-web structure can profoundly influence ecosystem properties [91].

In summary, the limitations in the ecological model of seamounts are possibly related to model simplification and other sources of data uncertainty. The configuration adopted in the AQUATOX model highly simplifies the real complex system that is a seamount and, due to their assumptions and gaps in data, model uncertainty is very relevant in this work. The nature of seamounts as they are deep sea systems and difficult to access, make sampling limited and the available datasets scarce for model development. The unavailability of extensive datasets for model parameterisation, calibration, and validation of the seamount food web, as well as the limited knowledge of seasonality, life cycle and ecology of most deep-sea species.

The aforementioned limitations in the trophic web model propagate to the simulations of HNS effects in seamounts. Ideally, the exploratory scenarios should be conducted after proper model validation against an independent dataset [92], which currently is not possible due to the unavailability of additional datasets.

On the other hand, besides the acute toxicology accounted for in the model (LC_{50}), other toxicological parameters should also be considered (e.g., chronic toxicology - EC_{50}) in more realistic representations, which would also benefit from existing toxicological parameters of the considered HNS for every functional group.

To tackle this limitation, it is essentially to conduct further ecotoxicological experiments and assess specific metabolic pathways of HNS on marine species, in this particular case, particularly, on deep-sea marine species over different life cycle stages and endpoints (e.g., chronic HNS effects, such as in reproduction, growth), as HNS effects may differ. This methodology would be key to fulfil data gaps, produce good quality datasets to support model development, calibration, validation and, then, bring together all these necessary requirements to run different scenarios to evaluate their effects in seamounts.

Interestingly but unexpectedly, AQUATOX predicts a decrease in oxygen concentration promoted by the breakdown of HNS, which in turn leads to the mortality of biotic groups that are strongly limited by dissolved oxygen concentrations, particularly, at higher depths. Although such results require validation, the indirect effect of pollutants degradation on oxygen depletion cannot be ruled out in case of HNS spills at sea.

Nonetheless, a reduction in metabolic activity with increasing depth would also probably decrease the endogenous production of reactive oxygen species [93], which can highly influence HNS dynamics and ecotoxicology in the inhabiting species of seamounts.

Other approaches may also play an important role, such as extending the sensitivity analyses on the AQUATOX model to identify critical parameters influencing the model's response to HNS exposure and oxygen depletion, which can help prioritise data collection and guide model improvements in terms of detailed biogeochemical processes and refining parameter values.

Attending to these limitations, we strongly suggest that application of the current model version should be limited to unravel useful insights for further research (i.e., point out the direction of future research, such as conducting research with more sensitive species to build a more profound knowledge on these and, thus, achieve a more robust model), rather than as a support decision tool. As mentioned, extensive improvements in dataset and potential model complexity must be enhanced to respond to the problematic explored in this work.

4.3. Menez Gwen ecosystem model

Regarding the Menez Gwen vent field ecosystem, the MG Ecopath model analysis provided insights into the characteristics and functioning of this deep-sea ecosystem. The food web structure exhibits simplicity with three trophic levels and low predation pressure, which is consistent with previous studies on deep-sea hydrothermal

vents [7, 94]. The "vent Mussels" group, despite being dominant in biomass, has non-trophic links with other consumers, as previously reported by [75, 95]. This fact is represented in the trophic web model, with the "vent mussels" group showing an EE value of 0, as it has no direct trophic links with other consumer species.

The model's physiological realism is demonstrated through the analysis of vital rates, in the PREBAL analysis, according to [61]. On the other hand, the model's Pedigree index indicates a model based on data of a reasonable quality. The simplified connectivity within the food web, as indicated by Omnivory Indexes, suggests functional redundancy among co-occurring species, contributing to ecosystem resilience. The keystone species identified by the model include "Free-living bacteria," highlighting their crucial role in shaping the ecosystem [96], which is in line with experimental evidence. Likewise, the MG ecosystem has shown to be in a developmental stage and has not yet reached maturity [97], as reflected by energy usage inefficiencies and low values of total system throughput and functional complementarity index. However, the ecosystem displays high productivity and shows potential for adaptation and stability in response to changes [98].

The simulations conducted in our study show that the hypothetical spills of 4NP, AN, and NTB, at the MG hydrothermal vent field, will not have observable impacts on the local benthic community. However, the simulation for the tetrachloroethylene (PCE) accidental spill shows that concentrations may surpass the acute toxicity levels for two functional groups in the MG trophic web, namely, "vent Gastropods" and "vent Mussels". As a consequence, these two functional groups suffer a 50% reduction in their biomass, which subsequently leads to several impacts on higher and lower trophic levels, namely:

- The reduction in "vent Gastropods'' negatively affects "vent Shrimps" and "vent Crabs," as these two groups rely on "vent Gastropods'' as an important food source, with a more noticeable effect on "vent Crabs" due to their higher trophic level. This indicates a potential trophic cascade effect of the HNS on the MG food web.

- The reduction in "vent Mussels" biomass, despite not directly serving as a nutritional resource in the vent field food web, has a positive effect on the density of their prey, particularly, on "free-living bacteria," which in turn benefits other trophic levels such as "Copepods." This illustrates a mediating effect associated with the reduction in "vent Mussels."

Nonetheless, despite the disturbances caused by PCE on the MG community, the results from the MG ecosystem model suggest that, 18 years after the simulated HNS spill incident, the ecosystem tends to recover its initial stability. However, the recovery of the foundation species, "vent Mussels," is slower and less pronounced compared to the other species. Since foundation species have a large effect on the community structure by modifying environmental conditions, species interactions and resource availability, their initial presence is required before the subsequent establishment of populations of other associated species [99]. Thus, *Bathymodiolus spp*., as the foundation species in Atlantic deep-sea vent ecosystems, can be used as metrics of the system's productivity and functioning [100].

4.3.1. Limitations of the Menez Gwen ecosystem model

It is important to note that the food web model used in our study does not consider non-trophic relationships, such as the engineering role of foundation species ("vent Mussels" in this case), which may influence the overall structure, stability, and functioning of the ecosystem [101]. Indeed, the engineering role of "vent Mussels" in creating complex habitats and their persistence even after death play a crucial role in the surrounding environment [102].

Notwithstanding, hydrothermal vents are subject to natural disturbance regimes such as volcanic eruptions and hydrothermal cycles, which can reset the system or affect biological productivity and community composition [103, 104]. Therefore, while our simulations suggest eventual recovery under the HNS spill scenario, it is essential to consider the potential cumulative effects of natural disturbances combined with anthropogenic impacts, which may exceed the resilience of the system for recovery.

Overall, the present results suggest that the severity of the impact of a HNS spill can vary depending on several factors, such as the specific characteristics of the HNS, the final concentration at the vent field, exposure duration, ocean conditions, and the sensitivity of the ecosystem [105]. Moreover, although the dispersion model indicates a complete leakage of the HNS from the sunk containers after 10 days for the tested scenarios, this can vary in a real incident as it depends on numerous factors (e.g., volume of containers, depth, pressure, temperature).

To sum up, the specific limitation of the MG model are:

- *P/B* rates for consumer groups were estimated using empirical equations (described by [54]), as well as their Q/B rates (according to the approach described in [106]);
- In the case of primary producers ("Free-living bacteria"), due to lack of data, EE and P/B values were based on other deep-sea ecosystem models [107-109]. Based on these values, the *B* of the "Free-living bacteria" was then estimated by Ecopath;
- The biomass of the detritus groups was also estimated based on data previously reposted for an EPR hydrothermal vent, at 1000-1300 m depth [107];
- The acute toxicity values of the four HNS (LC_{50} concentrations) used in the model are from proxy species, since there is no data available on the toxicity of 4NP, AN, PCE or NTB on the MG vent species. Because the proxy species are not deep-sea vent species, the used acute toxicity values do not account for the adaptations exhibited by vent organisms to living in these extreme habitats, namely, to toxic substances such as [110-113];
- The model does not take into account the bioaccumulation of contaminants that may be relevant for the ecosystem function and can have insidious effects, especially at higher trophic levels.

The results of the effects of the four HNS on the two studied deep-sea ecosystems must be regarded cautiously and, at this point, only as a theoretical exercise. In fact, if a protection factor of 100, 1000, 10000 or would be used to set the LC_{50} as frequently recommended in case of toxicity data gaps [114], the effects of the

studied HNS on both the seamount and the vent field ecosystems would be much stronger, potentially, leading to the extinction of the deep-sea communities. On the other hand, some of these organisms are adapted to extreme environmental conditions, including metal-enriched environments as is the case of the Atlantic deep-sea mussel (*Bathymodiolus sp*), and have developed mechanisms to cope with such extreme conditions (e.g., metallothioneins) [111]. We do not know if these adaptions would confer them some kind of protection against other type of pollutants.

5. CONCLUSIONS AND RECOMMENDATIONS

The numerical framework developed under the MODELRISK project is a model ensemble that incorporates an ocean circulation model (ROMS) calibrated for the study site (Azores region), a lagrangian model (OpenDrift) to describe the dispersion of four selected HNS after incident spills, an ecosystem model of a typical North Atlantic (NA) seamount (AQUATOX) and a food web model of the shallower North Atlantic (NA) deep sea vent field (Ecopath with Ecosim), to describe food web dynamics and the toxicological effects of HNS on the function of NA seamounts and deep sea vent fields (Figure 28).

While developing and assembling this numerical framework, we came up with a set of limitations and knowledge gaps that refrain the immediate use of this framework as a decision-support tool in case of accidental HNS spills at sea, namely:

- The absence of a numerical tool that describes the chemical transformations of HNS in the water (horizontally and vertically), while describing their dispersion (the version 1.0 of ChemicalDrift by OpenDrift has just been published [115]);
- Available ecosystem models are not, in general, appropriate to simulate chemosynthetic ecosystems and habitats (i.e., where energy is not produced by photosynthesis);

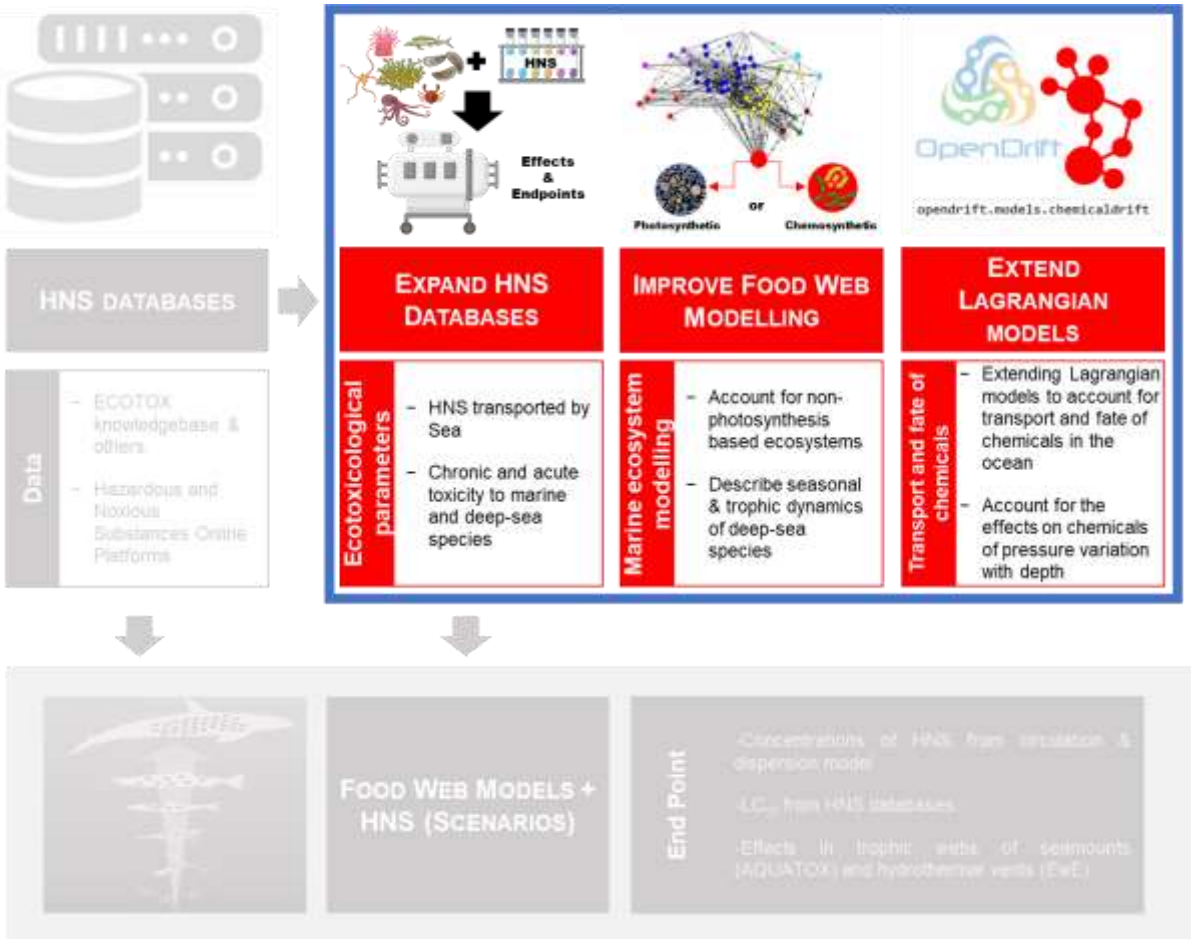

Figure 28. Recommended research efforts to tackle the limitations previously identified.

- There is a deep knowledge gap regarding chronic and acute toxicity of the most frequently transported HNS on marine and deep-sea species;
- Available knowledge regarding the ecology and physiology of some marine species and most deep-sea species is rather limited.

Hence, we recommend that research efforts may be carried to tackle the aforementioned points (Figure 28). Subsequently, modellers can improve the calibration, verification and, ultimately, the validation of the MODELRISK framework, allowing it to be used as a support tool in HNS spill response at Sea.

6. MODELRISK OUTPUTS & OUTREACH

Table 11. Dissemination of project results: MODELRISK outputs & outreach activities

Date	Activity	Type	Link/Observations
01/05/2021-31/10/2021	MODELRISK team supervised a 1-month internship of an undergraduate international student (Johannes Herzog - Universität Für Bodenkultur Wien), who developed activities within task 1 and task 2 of the project	Supervision	NA
01/05/2021-31/10/2021	MODELRISK is announced at CIIMAR home page and at CIIMAR social media	Dissemination	https://www2.ciimar.up.pt/projects.php?id=178
01/05/2022-31/07/2022	MODELRISK team supervised a 3-month internship of an undergraduate international student (Ombéline Harasse - SeaTech Engineering School, University of Toulon (France), who developed activities within the tasks 2 and 3 of the project	Supervision	This work is a collaboration between MODELRISK and DEEPRISK, another project in which the team is involved Title: *A modelling framework to assess multiple metals impacts on marine food webs: Relevance for assessing the ecological implications of deep-sea mining based on a systematic review*
04/05/2022	A talk presenting part of the work under development within MODELRISK was given at a national event organized by the Portuguese Navy	Presentation /Dissemination	Azevedo, A., Ramos, S., Amorim, F., Martins, I., 2022. *Numerical tools to support environmental risk assessment and management of accidents with pollutants spills at sea*. Presented at ATLANTIC POLEX.PT, Viana do Castelo (Portugal)

(continuation of Table 11)

Date	Activity	Type	Link/Observations
18/09/2022	Presenting to the general public research and results carried out within the MODELRISK project	Presentation/ Dissemination	https://www2.ciimar.up.pt/events.php?id=358
26/09/2022	Presenting MODELRISK project and preliminary results, in CIIMAR's annual meeting	Presentation/ Dissemination	Martins, I., 2022. MODELRISK- Ecosystem models to support Environmental Risk Assessment of marine ecosystems under HNS spills. Presented at CIIMAR, Matosinhos (Portugal)
27/10/2022	Invited talk to present MODELRISK project and preliminary results, in an online seminar	Presentation/ Dissemination	Martins, I., Azevedo, A., Guerra, A., Amorim, F., 2022. MODELRISK: Ecosystem models to support Environmental Risk Assessment of Marine Ecosystems under HNS spills. Presented online at Seminário Novos e Velhos Saberes, UFBA (Brazil)
27/11/2022	Invited talk to present the importance of ecological modelling in the scope of marine environmental risk assessment; presentation of MODELRISK project and preliminary results	Presentation/ Dissemination	Martins, I., 2022. O paradoxo do mar dos Açores: Ecossistemas icónicos numa das mais congestionadas rotas marítimas do mundo (in Portuguese). Presented at Fundação de Serralves, Porto (Portugal)
03/05/2023	Presentation of results of MODELRISK project in a Scientific Meeting	Poster presentation in an International Scientific Symposium/ Conference	Azevedo, A., Guerra, A., Martins, I., 2023. Modelling tools to support the conservation of seamount communities: scope, limitations and emergent challenges. The International Society for Ecological Modelling (ISEM), Toronto (Canada)

(continuation of Table 11)

Date	Activity	Type	Link/Observations
03/05/2023	Presentation of results of MODELRISK project in a Scientific Meeting	Poster presentation in an International Scientific Symposium/ Conference	Guerra, A., Azevedo, A., Colaço, A., Amorim F., Santos M.M., Martins, I., 2023. Modelling the impact of HNS spills on Atlantic deep-sea hydrothermal vents. The International Society for Ecological Modelling (ISEM), Toronto (Canada)
03/05/2023	Presentation of results of MODELRISK project in a Scientific Meeting	Oral presentation in an International Scientific Symposium/ Conference	Azevedo, A., Guerra, A., Amorim, F., Martins, I., 2023. Modelling the effects of Hazardous and Noxious Substances (HNS) throughout a typical seamount food web. The International Society for Ecological Modelling (ISEM), Toronto (Canada)
05/05/2023	Presentation of results of MODELRISK project in a Scientific Meeting	Oral presentation in an International Scientific Symposium/ Conference	Martins, I., Guerra, A., Azevedo, A., Xavier, C., Pinheiro, M., Santos, M.M., Colaço, A., Duarte, P., 2023. Using a DEB model to study the effects of deep-sea mining on endemic species from Atlantic deep-sea hydrothermal vents. The International Society for Ecological Modelling (ISEM), Toronto (Canada)
06/2023	Scientific paper resulting from the internship of the undergraduate international student Ombéline Harasse, within the MODELRISK project	Scientific paper in an indexed journal (Q1)	Martins, I.I., Guerra, A., Azevedo, A., Harasse, O., Colaço, A., Xavier, J., Caetano, M., Carreiro- Silva, M., Martins, I., Neuparth, T., Raimundo, J., Soares, J., Santos, M.M., 2023. A modelling framework to assess multiple metals impacts on marine food webs: Relevance for assessing the ecological implications of deep-sea mining based on a systematic review. Marine Pollution Bulletin, 191, 114902 https://www.sciencedirect.com/science/article/abs/pii/S0025326X23003338?via%3Dihub

(continuation of Table 11)

Date	Activity	Type	Link/Observations
28/06/2023	Update of an existent database, following the revision required to conduct MODELRISK tasks	Database	https://www.ciimar.up.pt/hns/

7. ACKNOWLEDGEMENTS

MODELRISK is financially supported by ITOPF as the beneficiary of the 10th ITOPF R&D Award.

We acknowledge the valuable comments, suggestions, and brainstorming from our team of consultants of OKEANOS DOP | University of Azores (Portugal), and from the accompanying ITOPF team (Angela Pinzon and Duarte Soares).

8. REFERENCES

1. Rogers, A., *Threats to Seamount Ecosystems and Their Management*. 2019. p. 427-451.
2. Rogers, A.D., *Environmental Change in the Deep Ocean*, in *Annual Review of Environment and Resources, Vol 40*, A. Gadgil and T.P. Tomich, Editors. 2015. p. 1-38.
3. Rogers, A.D., *Chapter Four - The Biology of Seamounts: 25 Years on*, in *Advances in Marine Biology*, C. Sheppard, Editor. 2018, Academic Press. p. 137-224.
4. Morato, T., et al., *Seamounts are hotspots of pelagic biodiversity in the open ocean.* Proceedings of the National Academy of Sciences of the United States of America, 2010. **107**(21): p. 9707-9711.
5. Morato, T., et al., *Evidence of a seamount effect on aggregating visitors.* Marine Ecology Progress Series, 2008. **357**: p. 23-32.
6. Jannasch, H.W. and M.J. Mottl, *Geomicrobiology of Deep-Sea Hydrothermal Vents.* Science, 1985. **229**(4715): p. 717-725.
7. Van Dover, C.L., et al., *Biogeography and Ecological Setting of Indian Ocean Hydrothermal Vents.* Science, 2001. **294**(5543): p. 818-823.
8. Dubilier, N., C. Bergin, and C. Lott, *Symbiotic diversity in marine animals: the art of harnessing chemosynthesis.* Nature Reviews Microbiology, 2008. **6**(10): p. 725-740.
9. Levin, L.A., et al., *Hydrothermal Vents and Methane Seeps: Rethinking the Sphere of Influence.* Frontiers in Marine Science, 2016. **3**.
10. Van Dover, C.L., *The Ecology of Deep-Sea Hydrothermal Vents*. 2000, Princeton: Princeton University Press.
11. Colman, D.R., et al., *Geobiological feedbacks and the evolution of thermoacidophiles.* The ISME Journal, 2018. **12**(1): p. 225-236.
12. Huber, H., et al., *Ignicoccus gen. nov., a novel genus of hyperthermophilic, chemolithoautotrophic Archaea, represented by two new species, Ignicoccus islandicus sp nov and Ignicoccus pacificus sp nov. and Ignicoccus pacificus sp. nov.* International Journal of Systematic and Evolutionary Microbiology, 2000. **50**(6): p. 2093-2100.
13. Rizzo, C., et al., *Ecological and Biotechnological Relevance of Mediterranean Hydrothermal Vent Systems.* Minerals, 2022. **12**(2): p. 251.
14. Miller, K.A., et al., *An Overview of Seabed Mining Including the Current State of Development, Environmental Impacts, and Knowledge Gaps.* Frontiers in Marine Science, 2018. **4**.
15. German, C.R., et al., *Deep-Water Chemosynthetic Ecosystem Research during the Census of Marine Life Decade and Beyond: A Proposed Deep-Ocean Road Map.* PLOS ONE, 2011. **6**(8): p. e23259.
16. *IMO approves draft Protocol to bring 1996 Hazardous and Noxious Substances (HNS) Convention into effect.* Marine Pollution Bulletin, 2009. **58**(6): p. 791-791.
17. Cho, H., et al., *Decision-making process for places of refuge in hazardous and noxious substances incident: Case study of South Korea.* Marine Policy, 2019. **108**.
18. Wan, S.Y., et al., *Emerging marine pollution from container ship accidents: Risk characteristics, response strategies, and regulation advancements.* Journal of Cleaner Production, 2022. **376**.
19. Cunha, I., S. Moreira, and M.M. Santos, *Review on hazardous and noxious substances (HNS) involved in marine spill incidents-An online database.* Journal of Hazardous Materials, 2015. **285**: p. 509-516.
20. Cunha, I., et al., *Fate, behaviour and weathering of priority HNS in the marine environment: An online tool.* Marine Pollution Bulletin, 2016. **111**(1-2): p. 330-338.
21. Fuhrer, M., et al., *Offshore experiments on styrene spillage in marine waters for risk assessment.* Marine Pollution Bulletin, 2012. **64**(7): p. 1367-1374.
22. Wu, J.Y., et al., *Study on Risk Assessment Methods and Zoning of Hazardous Chemicals Leaking into Seas.* International Journal of Environmental Research and Public Health, 2022. **19**(22).
23. Angelliaume, S., et al., *Multifrequency Radar Imagery and Characterization of Hazardous and Noxious Substances at Sea.* Ieee Transactions on Geoscience and Remote Sensing, 2017. **55**(5): p. 3051-3066.
24. Park, J.J., et al., *Detection of Toluene Hazardous and Noxious Substances (HNS) Based on Hyperspectral Remote Sensing.* Journal of the Korean Earth Science Society, 2021. **42**(6): p. 623-631.

25. Park, J.J., et al., *Estimation of hazardous and noxious substance (toluene) thickness using hyperspectral remote sensing.* Frontiers in Environmental Science, 2023. **11**.

26. Zhan, S.Y., et al., *Floating Xylene Spill Segmentation from Ultraviolet Images via Target Enhancement.* Remote Sensing, 2019. **11**(9).

27. Choi, J.S., et al., *Electrical and Chemical Sensing Properties of a Printed Indium-Tin-Oxide Film for the Detection of Hazardous and Noxious Substances.* Journal of the Korean Physical Society, 2020. **76**(11): p. 1005-1009.

28. Noh, J., et al., *Investigation on the Printed CNT-Film-Based Electrochemical Sensor for Detection of Liquid Chemicals.* Sensors, 2021. **21**(15).

29. Neuparth, T., et al., *Toxicity effects of Hazardous and Noxious Substances (HNS) to marine organisms: acute and chronic toxicity of p-xylene to the amphipode Gammarus locusta.* Journal of Toxicology and Environmental Health-Part a-Current Issues, 2014. **77**(20): p. 1210-1221.

30. Neuparth, T., et al., *Simulation of a Hazardous and Noxious Substances (HNS) spill in the marine environment: Lethal and sublethal effects of acrylonitrile to the European seabass.* Chemosphere, 2013. **93**(6): p. 978-985.

31. Wang, X.F., et al., *Toxicity evaluation of butyl acrylate on the photosynthetic pigments, chlorophyll fluorescence parameters, and oxygen evolution activity of Phaeodactylum tricornutum and Platymonas subcordiformis.* Environmental Science and Pollution Research, 2021. **28**(43): p. 60954-60967.

32. Wu, M.N., et al., *Impact of P-Chloroaniline on Oxidative Stress and Biomacromolecules Damage in the Clam Ruditapes philippinarums: A Simulate Toxicity Test of Spill Incident.* International Journal of Environmental Research and Public Health, 2022. **19**(9).

33. Zheng, L., et al., *Evaluating the toxic effects of three priority hazardous and noxious substances (HNS) to rotifer Brachionus plicatilis.* Environmental Science and Pollution Research, 2017. **24**(35): p. 27277-27287.

34. Wang, X.T. and F.P. Meng, *Emergency responses to acrylonitrile maritime spills from the perspective of marine ecological protection.* Frontiers in Marine Science, 2022. **9**.

35. Dong, B.Y. and L. Zhu, *Civil Liability and Compensation for Damage in Connection With the Carriage of Hazardous and Noxious Substances: Chinese Perspective.* Ocean Development and International Law, 2019. **50**(2-3): p. 209-224.

36. Zhuo, R.X., *The HNS Convention: will it be a game changer for China's marine pollution law?* Natural Resources Journal, 2020. **60**(2): p. 207-238.

37. Morato, T., et al., *Abundance and distribution of seamounts in the Azores.* Marine Ecology Progress Series, 2008. **357**: p. 17-21.

38. Marcon, Y., et al., *Megafaunal distribution and assessment of total methane and sulfide consumption by mussel beds at Menez Gwen hydrothermal vent, based on geo-referenced photomosaics.* Deep Sea Research Part I: Oceanographic Research Papers, 2013. **75**: p. 93-109.

39. Cerqueira, T., et al., *Microbial diversity in deep-sea sediments from the Menez Gwen hydrothermal vent system of the Mid-Atlantic Ridge.* Marine Genomics, 2015. **24**: p. 343-355.

40. Charlou, J.L., et al., *Compared geochemical signatures and the evolution of Menez Gwen (37°50'N) and Lucky Strike (37°17'N) hydrothermal fluids, south of the Azores Triple Junction on the Mid-Atlantic Ridge.* Chemical Geology, 2000. **171**(1): p. 49-75.

41. Desbruyères, D., et al., *Variations in deep-sea hydrothermal vent communities on the Mid-Atlantic Ridge near the Azores plateau.* Deep Sea Research Part I: Oceanographic Research Papers, 2001. **48**: p. 1325-1346.

42. Egbert, G. and S. Erofeeva, *Efficient Inverse Modeling of Barotropic Ocean Tides.* J. Atmos. Ocean. Tech., 2002. **19**: p. 183-204.

43. Saha, S., et al., *The NCEP climate forecast system reanalysis.* Bulletin of The American Meteorological Society - BULL AMER METEOROL SOC, 2010. **91**.

44. Tkalich, P. and E.S. Chan, *Vertical mixing of oil droplets by breaking waves.* Marine Pollution Bulletin, 2002. **44**(11): p. 1219-1229.

45. Galieriková, A., et al., *Study of maritime accidents with hazardous substances involved: comparison of HNS and oil behaviours in marine environment.* Transportation Research Procedia, 2021. **55**: p. 1050-1064.

46. Marta-Almeida, M., et al., *Dynamics of river plumes in the South Brazilian Bight and South Brazil.* Ocean Dynamics, 2021. **71**(1): p. 59-80.

47. Marta-Almeida, M., et al., *Fundão Dam collapse: Oceanic dispersion of River Doce after the greatest Brazilian environmental accident.* Marine Pollution Bulletin, 2016. **112**(1): p. 359-364.

48. Marta-Almeida, M., et al., *Efficient tools for marine operational forecast and oil spill tracking.* Marine Pollution Bulletin, 2013. **71**(1): p. 139-151.

49. Morato, T., et al., *Food-Web and Ecosystem Structure of the Open-Ocean and Deep-Sea Environments of the Azores, NE Atlantic.* Frontiers in Marine Science, 2016. **3**.

50. Clough, J.S., *AQUATOX (Release 3.2) - Modeling Environmental fate and ecological effects in aquatic ecosystems - User's manual, Office of Research and Development (ORD), United States Environmental Protection Agency (US EPA) - EPA/600/B-18/233. URL: https://www.epa.gov/sites/default/files/2018-09/documents/aquatox_uman_3.2.pdf [last access: 05 December 2022]*. 2018.

51. Park, R.A. and J.S. Clough, *AQUATOX (Release 3.2) - Modeling Environmental fate and ecological effects in aquatic ecosystems - Technical Documentation, Office of Research and Development (ORD), United States Environmental Protection Agency (US EPA) - EPA/600/B-18/241. URL: https://www.epa.gov/sites/default/files/2018-09/documents/aquatox_tech_doc_3.2.pdf [last access: 05 December 2022].* 2018.

52. Park, R.A., J.S. Clough, and M.C. Wellman, *AQUATOX: Modeling environmental fate and ecological effects in aquatic ecosystems.* Ecological Modelling, 2008. **213**(1): p. 1-15.

53. Park, R.A., et al., *Estimating fate and effects with the aquatic ecosystems model, AQUATOX.* Abstracts of Papers of the American Chemical Society, 1997. **213**: p. 33-CINF.

54. Brey, T., *Population dynamics in benthic invertebrates. A virtual handbook*, G. Alfred Wegener Institute for Polar and Marine Research, Editor. 2001.

55. Colaco, A., et al., *Ecology of the Menez Gwen hydrothermal vent field (Mid-Atlantic Ridge/Azores Triple Junction).* Cahiers De Biologie Marine, 1998. **39**: p. 237-240.

56. Sarrazin, J., et al., *Endogenous versus exogenous factors: What matters for vent mussel communities?* Deep Sea Research Part I: Oceanographic Research Papers, 2020. **160**: p. 103260.

57. Colaço, A., et al., *Bioaccumulation of Hg, Cu, and Zn in the Azores triple junction hydrothermal vent fields food web.* Chemosphere, 2006. **65**(11): p. 2260-2267.

58. Boschen-Rose, R.E. and A. Colaço, *Northern Mid-Atlantic Ridge Hydrothermal Habitats: A Systematic Review of Knowledge Status for Environmental Management.* Frontiers in Marine Science, 2021. **8**.

59. Christensen, V. and C.J. Walters, *Ecopath with Ecosim: methods, capabilities and limitations.* Ecological Modelling, 2004. **172**(2): p. 109-139.

60. Christensen, V., C. Walters, and D. Pauly, *Ecopath with Ecosim: A User's Guide.* Fisheries Centre, University of British Columbia, Vancouver, Canada and ICLARM, Penang, Malaysia, 2005. **12**.

61. Link, J.S., *Adding rigor to ecological network models by evaluating a set of pre-balance diagnostics: A plea for PREBAL.* Ecological Modelling, 2010. **221**(12): p. 1580-1591.

62. Gage, J.D. and P.A. Tyler, *Deep-Sea Biology: A Natural History of Organisms at the Deep-Sea Floor*. 1991: Cambridge University Press.

63. McNichol, J., et al., *Primary productivity below the seafloor at deep-sea hot springs.* Proceedings of the National Academy of Sciences, 2018. **115**(26): p. 6756-6761.

64. Walters, C., V. Christensen, and D. Pauly, *Structuring dynamic models of exploited ecosystems from trophic mass-balance assessments.* Reviews in Fish Biology and Fisheries, 1997. **7**(2): p. 139-172.

65. Walters, C., et al., *Representing Density Dependent Consequences of Life History Strategies in Aquatic Ecosystems: EcoSim II.* Ecosystems, 2000. **3**: p. 70-83.

66. Walters, C. and V. Christensen, *Adding realism to foraging arena predictions of trophic flow rates in Ecosim ecosystem models: Shared foraging arenas and bout feeding.* Ecological Modelling, 2007. **209**(2): p. 342-350.

67. De, J., A. Sarkar, and N. Ramaiah, *Bioremediation of toxic substances by mercury resistant marine bacteria.* Ecotoxicology, 2006. **15**(4): p. 385-389.

68. Maksimova, Y.G., A.Y. Maksimov, and V.A. Demakov, *Biofilms of nitrile-hydrolyzing bacteria: Dynamics of growth, resistance to toxic substances, and biotechnological potential.* Applied Biochemistry and Microbiology, 2016. **52**(8): p. 739-749.

69. Aguiar, A.L., et al., *Upwelling processes along the South Equatorial Current bifurcation region and the Salvador Canyon (13°S), Brazil.* Continental Shelf Research, 2018. **171**: p. 77-96.

70. Aguiar, A.L., et al., *Upwelling processes along a western boundary current in the Abrolhos–Campos region of Brazil.* Continental Shelf Research, 2014. **85**: p. 42-59.

71. Amorim, F.N., et al., *The seasonal circulation of the Eastern Brazilian shelf between 10°S and 16°S: A modelling approach.* Continental Shelf Research, 2013. **65**: p. 121-140.

72. Clavel-Henry, M., et al., *Modeled buoyancy of eggs and larvae of the deep-sea shrimp Aristeus antennatus (Crustacea: Decapoda) in the northwestern Mediterranean Sea.* PLOS ONE, 2020. **15**(1): p. e0223396.

73. Pires, R.F.T., Á. Peliz, and A. dos Santos, *Into the deep – Dispersal models for deep-water decapod shrimp larvae: The case of Parapenaeus longirostris.* Progress in Oceanography, 2021. **194**: p. 102568.

74. Pauly, D. and V. Christensen, *Primary production required to sustain global fisheries.* Nature, 1995. **374**(6519): p. 255-257.

75. De Busserolles, F., et al., *Are spatial variations in the diets of hydrothermal fauna linked to local environmental conditions?* Deep Sea Research Part II: Topical Studies in Oceanography, 2009. **56**(19): p. 1649-1664.

76. Angelini, R., *Introdução ao modelo ECOPATH: descrição dos parâmetros de entrada e principais atributos ecossistêmicos. In: Angelini, R., Araújo, J.N., Falcão, A.P.C., editores. Modelagem Ecossistêmica para integração e manejo na Bacia de Campos (Atlântico Sudoeste). Rio de Janeiro: Elsevier. Habitats, v. 8. p. 9-23*. 2017. p. 9-23.

77. Stenstrom, M.K. and R.A. Poduska, *The effect of dissolved oxygen concentration on nitrification.* Water Research, 1980. **14**(6): p. 643-649.

78. Morato, T., C. Bulman, and T.J. Pitcher, *Modelled effects of primary and secondary production enhancement by seamounts on local fish stocks.* Deep Sea Research Part II: Topical Studies in Oceanography, 2009. **56**(25): p. 2713-2719.

79. Tecchio, S., M. Coll, and F. Sardà, *Structure, functioning, and cumulative stressors of Mediterranean deep-sea ecosystems.* Progress in Oceanography, 2015. **135**: p. 156-167.

80. Bradford-Grieve, J.M., et al., *Pilot trophic model for subantarctic water over the Southern Plateau, New Zealand: a low biomass, high transfer efficiency system.* Journal of Experimental Marine Biology and Ecology, 2003. **289**(2): p. 223-262.

81. Ekelund, R., et al., *Bioaccumulation of 4-nonylphenol in marine animals— A re-evaluation.* Environmental Pollution, 1990. **64**(2): p. 107-120.

82. Vidal-Liñán, L., et al., *Bioaccumulation of 4-nonylphenol and effects on biomarkers, acetylcholinesterase, glutathione-S-transferase and glutathione peroxidase, in Mytilus galloprovincialis mussel gills.* Environmental Pollution, 2015. **200**: p. 133-139.

83. Wang, L., et al., *Photodegradation of aniline in aqueous suspensions of microalgae.* Journal of Photochemistry and Photobiology B: Biology, 2007. **87**(1): p. 49-57.

84. Bingli, L., et al., *Prediction of the environmental fate and aquatic ecological impact of nitrobenzene in the Songhua River using the modified AQUATOX model.* Journal of Environmental Sciences, 2008. **20**(7): p. 769-777.

85. van Veen, F., *Food webs.* Current biology : CB, 2009. **19**: p. R281-3.

86. Denda, A. and B. Christiansen, *Zooplankton at a seamount in the eastern Mediterranean: distribution and trophic interactions.* Journal of the Marine Biological Association of the United Kingdom, 2011. **91**(1): p. 33-49.

87. Annasawmy, P., et al., *Stable isotope patterns of mesopelagic communities over two shallow seamounts of the south-western Indian Ocean.* Deep Sea Research Part II: Topical Studies in Oceanography, 2020. **176**: p. 104804.

88. Alt, J.C. and W.C. Shanks, *Stable isotope compositions of serpentinite seamounts in the Mariana forearc: Serpentinization processes, fluid sources and sulfur metasomatism.* Earth and Planetary Science Letters, 2006. **242**(3-4): p. 272-285.

89. Colaco, A., et al., *Trophodynamic studies on the Condor seamount (Azores, Portugal, North Atlantic).* Deep-Sea Research Part Ii-Topical Studies in Oceanography, 2013. **98**: p. 178-189.

90. Nishida, K., et al., *Prey use by three deep-sea fishes in the Emperor Seamount waters, North Pacific Ocean, as revealed by stomach contents and stable isotope analyses.* Environmental Biology of Fishes, 2016. **99**(4): p. 335-349.

91. Thébault, E. and M. Loreau, *Food-web constraints on biodiversity–ecosystem functioning relationships.* Proceedings of the National Academy of Sciences, 2003. **100**(25): p. 14949-14954.

92. Salciccioli, J.D., et al., *Sensitivity Analysis and Model Validation*, in *Secondary Analysis of Electronic Health Records*, M.I.T.C. Data, Editor. 2016, Springer International Publishing: Cham. p. 263-271.

93. Rees, J.-F., et al., *The Origins of Marine Bioluminescence: Turning Oxygen Defence Mechanisms Into Deep-Sea Communication Tools.* Journal of Experimental Biology, 1998. **201**(8): p. 1211-1221.

94. Portail, M., et al., *Food-Web Complexity in Guaymas Basin Hydrothermal Vents and Cold Seeps.* PLOS ONE, 2016. **11**(9): p. e0162263.

95. Portail, M., et al., *Food-web complexity across hydrothermal vents on the Azores triple junction.* Deep Sea Research Part I: Oceanographic Research Papers, 2018. **131**: p. 101-120.

96. Bergquist, D.C., et al., *Using stable isotopes and quantitative community characteristics to determine a local hydrothermal vent food web.* Marine Ecology-progress Series - MAR ECOL-PROGR SER, 2007. **330**: p. 49-65.

97. Odum, E.P., *The Strategy of Ecosystem Development.* Science, 1969. **164**(3877): p. 262-270.

98. Angelini, R., *Bases para a aplicação da teoria da informação em ecossistemas, com ênfase na ascendência.* Acta Scientiarum. Biological Sciences, 2002. **24**: p. 275-283.

99. Bruno, J. and M. Bertness, *Habitat modification and facilitation in benthic marine communities*. 2001. p. 201-218.

100. Angelini, C., et al., *Interactions among Foundation Species and Their Consequences for Community Organization, Biodiversity, and Conservation.* BioScience, 2011. **61**: p. 782-789.

101. Ellison, A.M., *Foundation Species, Non-trophic Interactions, and the Value of Being Common.* iScience, 2019. **13**: p. 254-268.

102. Lartaud, F., et al., *Fossil clams from a serpentinite-hosted sedimented vent field near the active smoker complex Rainbow, MAR, 36°13'N: Insight into the biogeography of vent fauna.* Geochemistry, Geophysics, Geosystems, 2010. **11**(8).

103. Van Dover, C.L., *Impacts of anthropogenic disturbances at deep-sea hydrothermal vent ecosystems: A review.* Marine Environmental Research, 2014. **102**: p. 59-72.

104. Whittaker, R.J., K.A. Triantis, and R.J. Ladle, *A General Dynamic Theory of Oceanic Island Biogeography: Extending the MacArthur- Wilson Theory to Accommodate the Rise and Fall of Volcanic Islands*, in *The Theory of Island Biogeography Revisited*, B.L. Jonathan and E.R. Robert, Editors. 2010, Princeton University Press: Princeton. p. 88-115.

105. Cho, H., et al., *Decision-making process for places of refuge in hazardous and noxious substances incident: Case study of South Korea.* Marine Policy, 2019. **108**: p. 103643.

106. Angelini, R., et al., *Ecosystem modeling as a framework to convert a multi-disciplinary research approach into a useful model for the Araçá Bay (Brazil).* Ocean & Coastal Management, 2018. **164**: p. 92-103.

107. Bell, J.B., C. Woulds, and D.v. Oevelen, *Hydrothermal activity, functional diversity and chemoautotrophy are major drivers of seafloor carbon cycling.* Scientific Reports, 2017. **7**(1): p. 12025.

108. Lein, A.Y., & Pimenov, N. V. (2002). , *Role of bacterial production at active hydrothermal fields in the total balance of organic carbon in the ocean. Biology of Hydrothermal Systems.* KMK Press, Moscow, 2002: p. 320-328.

109. Lin, Z.-Y., H.-W. Chen, and H.-J. Lin, *Trophic model of a deep-sea ecosystem with methane seeps in the South China Sea.* Deep Sea Research Part I: Oceanographic Research Papers, 2020. **159**: p. 103251.

110. Alayse-Danet, A.M., D. Desbruyères, and F. Gaill, *The possible nutritional or detoxification role of the epibiotic bacteria of Alvinellid polychaetes: Review of current data.* Symbiosis, 1987. **4**: p. 51-62.

111. Company, R., et al., *Adaptation of the antioxidant defence system in hydrothermal-vent mussels (Bathymodiolus azoricus) transplanted between two Mid-Atlantic Ridge sites.* Marine Ecology, 2007. **28**(1): p. 93-99.

112. Cosson-Mannevy, M.A., Cosson, R. P., Gaill, F., Laubier, L., *Transfert, accumulation et régulation des éléments minéraux chez les organismes des sources hydrothermales.* Oceanologica Acta, Special issue, 1988.

113. Vetter, R.D., et al., *Sulfide Detoxification by the Hydrothermal Vent Crab Bythograea thermydron and Other Decapod Crustaceans.* Physiological Zoology, 1987. **60**(1): p. 121-137.

114. Soares, J., et al., *Environmental risk assessment of accidental marine spills: A new approach combining an online dynamic Hazardous and Noxious substances database with numerical dispersion, risk and population modelling.* Science of the Total Environment, 2020. **715**.

115. Aghito, M., et al., *ChemicalDrift 1.0: an open-source Lagrangian chemical-fate and transport model for organic aquatic pollutants.* Geosci. Model Dev., 2023. **16**(9): p. 2477-2494.